

# Preferential orientation of floaters drifting in water waves

Wietze Herreman<sup>1</sup>†, Basile Dhoté<sup>1</sup>, Lucile Danion<sup>1</sup>,  
and Frédéric Moisy<sup>1</sup>

<sup>1</sup>Université Paris-Saclay, CNRS, FAST, 91405, Orsay, France.

(Received xx; revised xx; accepted xx)

Elongated floaters drifting in propagating water waves slowly rotate towards a preferential state of orientation. Short and heavy floaters tend to align longitudinally, along the direction of wave propagation, whereas long and light floaters align transversely, parallel to the wave crests and troughs. We investigate this phenomenon for homogeneous parallel-piped floaters by combining laboratory experiments with numerical simulations and asymptotic theory. For floaters small with respect to wavelength and for low amplitude waves, we show that the floater orientation is controlled by the non-dimensional number  $F = kL_x^2/\beta L_z$ , with  $k$  is the wavenumber,  $\beta$  the floater-to-water density ratio, and  $L_x$  and  $L_z$  the floater length and thickness. Theory places the longitudinal-transverse transition at the critical value  $F_c = 60$ , in fair agreement with the experiments. Using a simplified physical model, we elucidate the physical origin of the preferential orientation. Through its motion, the floater probes the velocity gradients along its surface. Next to a small mean displacement (Stokes drift), this results in a net torque which, for short floaters, always favors the longitudinal orientation. This net torque arises from a phase correlation between the instantaneous buoyancy torque and the instantaneous yaw angle of the floater, a mechanism analogous to the Kapitza pendulum. The transverse equilibrium of longer floaters has a different origin and arises from the variation of the submersion depth along their long axis. This varying submersion significantly increases the torque in the trough positions, when the tips are more submersed, and always pushes towards the transverse orientation.

**Key words:**

---

## 1. Introduction

The motion of a floating body in gravity waves is a classical problem in fluid mechanics with evident applications in the domain of naval engineering (Faltinsen 1993; Newman 2018; Falnes & Kurniawan 2020). At first order in wave magnitude, waves cause harmonic oscillations of the floating body in all six degrees of freedom, both linear (heave, surge, sway) and angular (pitch, roll, yaw). At second order, waves also cause a mean drift force and yaw moment on the body that affect surge, sway and yaw angle on long time-scales. For small isotropic floaters, this mean motion reduces to the classical Stokes drift in the direction of the wave propagation (Stokes 1847; van den Bremer & Breivik 2018; Calvert *et al.* 2021), a problem that received considerable interest for the modeling of pollutant transport in the oceans (Suaria *et al.* 2021; Yang *et al.* 2023; Sutherland *et al.* 2023).

† Email address for correspondence: wietze.herreman@universite-paris-saclay.fr

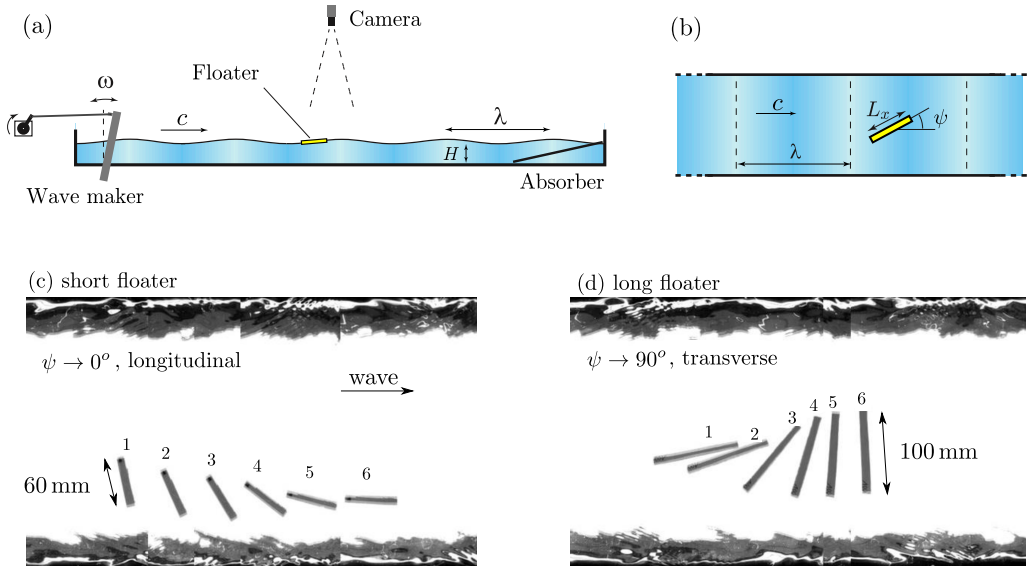


FIGURE 1. Experimental setup and chronophotographies. (a) Side view. Waves are generated in a water channel, of length 3 m and filled at height  $H = 10$  cm. (b) Top View. Floater of length  $L_x$ , making an angle  $\psi$  with the direction of wave propagation. (c-d) Chronophotographies, obtained by superimposing images acquired every wave period, for a wave length  $\lambda = 29$  cm and wave slope  $\epsilon = ak = 0.16$ . The short floater (length  $L_x = 60$  mm) gradually aligns in the direction of wave propagation (c), while the long floater ( $L_x = 100$  mm) aligns parallel to the wave crests (d).

For larger floaters of arbitrary shape, such as ships and floating structures, an angular drift can change the floater's orientation with respect to the wave incidence and this slow reorientation can in turn modify its linear drift. The combined linear and angular drifts are key features in sea keeping and maneuvering, and their modeling has been the subject of numerous works (Faltinsen 1993; Skejic & Faltinsen 2008; Newman 2018). In this paper, we are interested in the slow, second order yaw motion of elongated floaters drifting in gravity waves and how a preferential state of orientation spontaneously emerges.

Research on this topic started more than a century ago, with Suyehiro (1921) who first reported how small boat models displaced by propagating gravity waves rotate towards a preferential state of orientation with respect to the direction of incidence. Suheyiro believed that this was due to gyrostatic torques and hence of purely solid-mechanical origin. Newman disagreed with this and proposed in 1967 his famous article on the mean drift force and yaw moment due to waves (Newman 1967). Starting from a global momentum and torque balance, he expresses the second order drift force and yaw moment in terms of the *far-field* hydrodynamic wave potential (Kochin functions). Using slender body theory, he was able to calculate this far-field potential and hence to derive the first explicit formula for the second order yaw moment. This mean torque compared reasonably well with the experimental data of Spens & Lalangas (1962) (reproduced in Newman (1967)).

A key prediction of Newman's theory is that slender floating structures of length shorter than the wave-length should always be stable in *beam seas*, meaning that they will prefer to have their long axis parallel to the wave crests. In figure 1 we show two chronophotographs from our laboratory experiments that disagree with this prediction. Here, small homogeneous parallelepipeds of centimeter scale are left adrift in a propagating

wave in a 3-m long water tank, and pictures synchronized with the wave period are taken from above (details are given in section 2). In just a few wave periods, we observe that long floaters align parallel to the wave crests ('beam sea',  $\psi \rightarrow 90^\circ$ ), in agreement with Newman's prediction, but shorter floaters align along the direction of wave propagation ('head sea',  $\psi \rightarrow 0^\circ$ ); here  $\psi$  is the yaw angle between the floater long axis and the direction of wave propagation. Hence, it seems that preferential orientation, and by extension the mean second order yaw moment, may depend more subtly on the floater length and density. The main objective of this article is to clarify what physically governs this preference and to locate where the longitudinal-transverse transition occurs for floaters small with respect to the wavelength.

Since Newman's pioneering work, other groups have studied the second order yaw moment acting on floating bodies. The work of Salvesen (1974) is a simplification of Newman's model in which the floater is considered as a weak scatterer of the incoming wave. In Kashiwagi (1992) and Kashiwagi & Ohkusu (1993), Parseval's theorem is used to evaluate the mean drift force and yaw moment, instead of the method of stationary phase used by Newman. An entirely different, *near-field approach*, of direct pressure integration was proposed by Faltinsen (1980). These different methods are compared in Skejic & Faltinsen (2008), and show consistent results. Chen (2007) proposed a third method, the so-called *middle field formulation*, to compute mean wave loads on structures. This method, in which the potential is determined using a boundary element method, is implemented in the software pack Hydrostar (Bureau-Veritas 2016) that is commonly used in naval engineering applications. The experimental study of Le Boulluec *et al.* (2008) on drifting cargo containers briefly mentions the fact that containers can drift either in longitudinal positions (head-seas) or transverse position (beam-seas). Recently, Yasukawa *et al.* (2019) compared theory to new experimental measurements on a particular ship model. According to the authors, it remains difficult to make the theory and experiments for the mean yaw moment match well.

In this article, we propose a combined experimental, numerical and theoretical study on the preferential orientation of a model floater (homogeneous parallelepiped) drifting in a propagating gravity wave. Our model is based on the Froude-Krylov assumption and hence ignores all wave diffraction and wave radiation effects (no added mass, no radiation impedance). In spite of this simplicity, this model predicts a mean yaw moment in the limit of small floater length/wavelength ratio that is fully compatible with Newman's classical result (Newman 1967) and nearly in perfect agreement with mean yaw moment calculations of Chen (2007). Moreover, our simplified model also allows us to provide a simple physical picture for the origin of this preferential orientation.

The article is structured as follows. In section 2, we present a systematic series of experiments investigating the preferential orientation of floaters of varying length and density. In section 3, we define a simplified model in which we calculate the non-linear motion of the floater using a Froude-Krylov approximation. We show that numerical solutions of this model reproduce well the observed state of preferential orientation in our experiments. In section 4, we propose an asymptotic solution to our Froude-Krylov model in the double limit of small wave and small floater size. This yields the following, idealized evolution equation for the average yaw angle  $\bar{\psi}$ ,

$$\ddot{\bar{\psi}} \approx -\epsilon^2 \sin \bar{\psi} \cos^3 \bar{\psi} \left(1 - \frac{F}{F_c}\right). \quad (1.1)$$

This equation depends on two non-dimensional numbers: the wave-slope  $\epsilon = ka$  (with  $k$

the wavenumber and  $a$  the wave amplitude) and the number  $F$ , defined as

$$F = \frac{kL_x^2}{\beta L_z}, \quad (1.2)$$

with  $L_x, L_z$  the floater length and thickness and  $\beta$ , the floater-to-water density ratio. We recognise  $\bar{h} = \beta L_z$  as the equilibrium submersion depth or *draft* of our parallelepiped floaters. This idealised, dissipation-less evolution equation certainly does not capture all the complexity of realistic slow yawing, but it provides insight into the preferential state of orientation. It shows that, for  $F < F_c$ , the longitudinal position  $\bar{\psi} = 0^\circ$  is stable and hence preferred, whereas for  $F > F_c$ , the transverse position  $\bar{\psi} = 90^\circ$  is stable. Our theory predicts a transition at  $F_c = 60$ , in fair agreement with the experimental value  $F_c \simeq 45 \pm 10$ .

Our theory follows a 'near-field approach', but different from that of Faltinsen (1980), in the fact that it uses the Froude-Krylov approximation, which allows more analytical evaluation. In section 5, we finally derive the same model using a more simple physical procedure. This allows us to better understand what physically controls the preferential orientation. The longitudinal equilibrium position is due to an effective torque that appears as the floater probes low and high pressure regions while going through its first order motion. We show that this part of the torque creates a motion that is analogous to that of classical Kapitza pendulum, a pendulum whose anchor point is rapidly vibrated (Kapitza 1951; Landau & Lifschitz 1960; Butikov 2001). The transverse state of orientation is on the other hand due to the fact that long floaters have a variable submersion along their length. This variable submersion significantly enhances the instantaneous yaw moment in trough positions that always favors the transverse position. In Newman's model, only this second part of the torque is present, which explains why he found elongated structures to be stable in beam seas. Finally, in Sec. 6, we compare the analytical formula for the mean yaw moment in our theory to previous results obtained by Newman (1967) and Chen (2007). The agreement is surprisingly good, in particular when considering that we use a Froude-Krylov assumption in our model.

## 2. Experiments

A series of laboratory experiments with centimeter-scale floaters of varying size and density have been performed in a water flume. The experimental setup, sketched in figure 1(a-b), consists in a tank of length 3 m, width 0.38 m, filled with water at height  $H = 0.1$  m. Waves are generated by a wavemaker consisting in a paddle oscillating at frequency  $\omega/2\pi$  between 1 and 4 Hz, and are absorbed at the other end of the channel by a sloping plate.

We determine the wave profile  $\zeta(x, t)$  by imaging the instantaneous contact line through the lateral channel wall and using a line detection algorithm. The wave profile is well described by a simple sinus law,  $\zeta = a \cos(kx + \varphi(t))$ , with  $\varphi(t)$  the wave phase, from which we measure the wave amplitude  $a$  and wave number  $k = 2\pi/\lambda$  with precision  $\simeq 5\%$ . The measured wave number matches the dispersion relation in the gravity regime,  $\omega^2 = gk \tanh(kH)$ , with wave lengths  $\lambda$  in the range 10 – 82 cm. Experiments for wavelengths of the order of the channel width are discarded because resonant transverse sloshing modes are excited. We work in the weakly nonlinear wave regime, for wave slopes  $\epsilon = ak$  between 0.02 and 0.23.

The floaters are homogeneous rectangular parallelepipeds with length  $L_x$  between 20 and 140 mm, width  $L_y = 10$  mm and height  $L_z$  between 5 and 10 mm, cut from expanded PVC or polystyrene boards of various densities. We denote  $M$  the floater mass,  $\rho_s =$

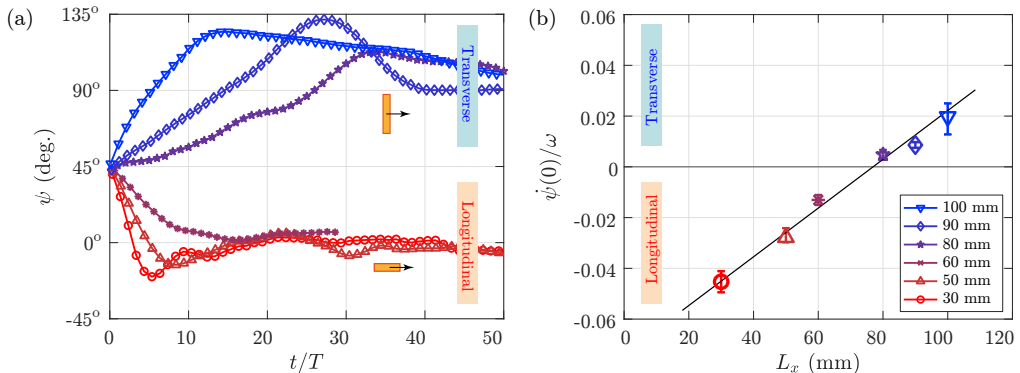


FIGURE 2. (a) Yaw angle  $\psi$  as a function of the time normalized by the wave period, for floaters of various lengths  $L_x$ . The time origin is chosen such that  $\psi(0) = 45^\circ$ . Wave frequency  $f = 2.3$  Hz, wavelength  $\lambda = 0.29$  m, wave slope  $ak = 0.16$ , floater waterline depth  $\bar{h} = 2.2$  mm. (b) Normalized angular velocity  $\dot{\psi}/\omega$  of the floater as a function of  $L_x$ .

$M/(L_x L_y L_z)$  its density, and  $\beta = \rho_s/\rho$  the floater-to-water density ratio. The floater size is large enough for the capillary effects to be negligible: the vertical component of the capillary force is less than 10% of the floater weight.

For each run, a floater is gently deposited at the surface of water at a distance  $x_0 \simeq 0.8$  m from the wave maker, with an initial yaw angle  $\psi_0$  of approximately  $45^\circ \pm 15^\circ$  from the  $x$  axis (controlling precisely  $\psi_0$  is difficult because the phase of the wave is not known at the time the floater is released). The floaters are imaged by a camera located above the wave tank. Using a tracking algorithm (library Tracker in Python), we measure the center of mass  $x_c(t)$  and the yaw angle  $\psi(t)$  of the floater on each frame. For each run, the floater is left adrift for about 1 m, and only trajectories staying approximately along the center line of the channel are retained to discard possible interaction with the side walls.

At first order, the floater motion is a combination of a back-and-forth oscillation of its center of mass, of amplitude given by the typical horizontal excursion of the fluid particle trajectories ( $\Delta x = a/\tanh(kH)$  for waves in finite depth) and angular oscillations. Superimposed to these fast oscillations are a slow drift of the center of mass in the direction of the wave propagation (Stokes drift) and a slow drift of the yaw angle, either towards the longitudinal ( $\psi = 0^\circ$ , denoted ‘L’) or transverse ( $\psi = 90^\circ$ , denoted ‘T’) orientation. To filter out the fast oscillations and focus on the slow dynamics of  $\psi$ , we synchronize the image acquisition with the wave maker oscillation, as illustrated in the chronophotographies of figure 1(c-d).

We first consider a set of floaters with a density ratio  $\beta = \rho_s/\rho = 0.44$  and thickness  $L_z = 5$  mm (expanded PVC foam boards ‘Forex’), and investigate the influence of the floater length  $L_x$ , for a fixed wavelength  $\lambda = 290$  mm and wave amplitude  $a = 7.4$  mm (wave slope  $\epsilon = ka = 0.16$ ). The time evolution of the yaw angle  $\psi$  is shown in figure 2(a). Because of the uncertainty on the initial angle  $\psi_0$ , we shift the time origin so that  $\psi = 45^\circ$  at  $t = 0$  for each run. The curves clearly separate in two groups, with small floaters ( $L_x \leq 60$  mm) tending to  $\psi = 0^\circ$  (longitudinal) and long floaters ( $L_x \geq 80$  mm) tending to  $\psi = 90^\circ$  (transverse). While short floaters precisely align in the longitudinal direction, with  $\psi \simeq 0 \pm 5^\circ$  at large time, long floaters show larger variations around  $\psi \simeq 90 \pm 30^\circ$ . These larger excursions can be due to the fact that long floaters are more subject to interactions with the side walls and to residual inhomogeneities in the mean flow.

The reorientation dynamics is faster for very short or very long floaters: they reach their

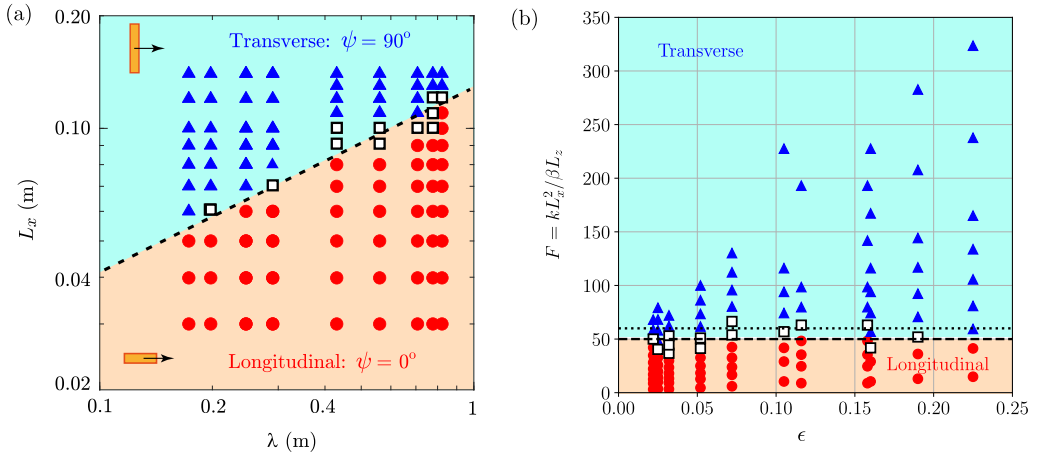


FIGURE 3. (a) Asymptotic floater orientation as a function of  $L_x$  and wavelength  $\lambda$ , for floaters with density  $\beta = 0.44$ , width  $L_y = 10$  mm and thickness  $L_z = 5$  mm. Red circles: longitudinal; Blue triangles: transverse. Black squares indicate erratic oscillations of the floater angle or non-reproducible experiments. The separation line is  $L_x = \sqrt{\ell\lambda}$ , with  $\ell \simeq 16 \pm 3$  mm. (b) Same data in the plan  $(F, \epsilon)$ , demonstrating the independence of the orientation with the wave steepness  $\epsilon$ . The long dashed line shows the experimental transition at  $F_c \simeq 50$ , and the short dashed line the theoretical prediction at  $F_c = 60$ .

asymptotic orientation after approximately 5 wave periods only, while the convergence is much slower (at least 20 wave periods) for intermediate lengths. This convergence rate is illustrated in figure 2(b) for various floater lengths, showing the angular velocity  $\dot{\psi}$  measured at  $t = 0$  normalized by the wave frequency  $\omega$  (this ratio measures the fraction of complete turn performed by the floater during one wave period). For this particular floater density and thickness,  $\dot{\psi}/\omega$  crosses zero for  $L_x \simeq 75$  mm, which defines the critical length  $L_{xc}$  separating the longitudinal and transverse orientations. Because of the slow dynamics at the crossover, the orientation is very sensitive to any experimental uncertainty for  $L_x$  close to  $L_{xc}$ , such as the precise choice of the initial angle  $\psi_0$ , inhomogeneities in the streaming flow, or small defects in the wetting line.

We have systematically determined the asymptotic yaw angle for various floater lengths  $L_x$ , wave lengths  $\lambda$  and amplitudes  $a$ . The preferential orientation of the floaters is first summarized in the plan  $(L_x, \lambda)$  in figure 3(a). When the asymptotic angle is  $\psi \simeq 0 \pm 10^\circ$ , floaters are labeled as ‘‘longitudinal’’ (red circles), and when  $\psi \simeq 90 \pm 30^\circ$  they are labeled as ‘‘transverse’’ (blue triangles). Floaters with indistinct orientation are marked with a black square. This diagram shows a clear separation between the longitudinal and transverse orientations, with a transition line well described by a square-root law,  $L_{xc} \simeq \sqrt{\ell\lambda}$ , with  $\ell \simeq 16 \pm 3$  mm a fitting parameter.

This square-root law nicely conforms to the prediction of the asymptotic theory presented in the next section, which demonstrates that the preferential orientation is independent of the wave slope  $\epsilon = ka$  and governed by the non-dimensional number  $F = kL_x^2/\beta L_z$ , with a longitudinal-transverse transition at  $F_c = 60$ . To check these predictions, we plot in figure 3(b) the same data in the  $(F, \epsilon)$  plane. We observe a clear separation between the longitudinal and transverse orientations, delimited by the line  $F \simeq 50$ , in fair agreement with the theory.

To further test the theory, we performed additional experiments with different floater densities  $\beta$  and thicknesses  $L_z$ , covering a range of immersion depths  $\bar{h} = \beta L_z$  between 1.8 and 5.3 mm. For each wavelength  $\lambda$ , we determine the critical floater length  $L_{xc}$

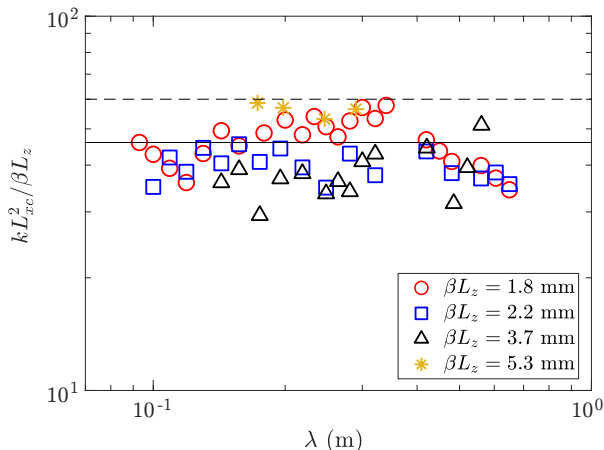


FIGURE 4. Critical values of  $F = kL_x^2/\beta L_z$  for the L-T transition as a function of the wavelength, for floaters of various densities  $\beta$  and thicknesses  $L_z$ . Solid line: average value  $F \simeq 45 \pm 10$ . Dashed line: theoretical prediction  $F_c = 60$ .

separating the longitudinal and transverse orientation, defined as the average between the largest longitudinal and smallest transverse floaters (the uncertainty on  $L_{xc}$  is 10 mm). Figure 4 summarizes the values of  $F$  at the transition as a function of the wavelength, yielding again a constant value,  $F \simeq 45 \pm 10$ . We can conclude that the two key predictions of the theory (floater orientation governed by  $F$  and independent of the wave slope  $\epsilon$ ) are well verified by our experiments.

### 3. Inviscid Froude Krylov model

To model the preferential state of orientation, we could in principle compute the mean yaw moment using existing models, either using the far-field approach of Newman (1967), the near-field approach of Faltinsen (1980) or the middle-field approach of Chen (2007). Here, we derive a more basic numerical model for idealised floater motion, that is based on the Froude-Krylov assumption. We demonstrate that this model reproduces well our experimental observations and hence, that it contains much of the essential physics.

#### 3.1. Simplifying assumptions

The idealised model that we will use to explain preferential orientation relies on the following simplifying assumptions:

(i) The incoming wave is a linear, inviscid potential gravity wave in deep water – The linearity assumption is reasonably satisfied in the experiments (maximum wave slope  $\epsilon = ka = 0.23$ ); the deep-water assumption is not fully satisfied ( $\tanh(kH) \simeq 0.65$  for the largest wave-length), but this is not essential to the theory.

(ii) Viscosity is negligible – The viscous stress on the floater is of the order  $\eta a \omega / \delta_s$ , where  $\delta_s = (\nu/\omega)^{1/2}$  is the thickness of the Stokes boundary layer. This viscous stress is much smaller than the wave pressure variations,  $p \sim \rho a \omega^2 / k$ , for  $\nu k^2 / \omega \ll 1$ , which is well satisfied in the experiments:  $\nu k^2 / \omega < 2 \times 10^{-4}$ .

(iii) Capillarity is negligible – The capillary length,  $\ell_c = \sqrt{\rho g / \gamma} \simeq 2$  mm (with  $\gamma$  the surface tension), is smaller than the characteristic floater size in our experiments. Note however that the meniscus at the rim of the floater likely creates an effective shape and may also weakly change the equilibrium immersion depth  $\bar{h}$ .

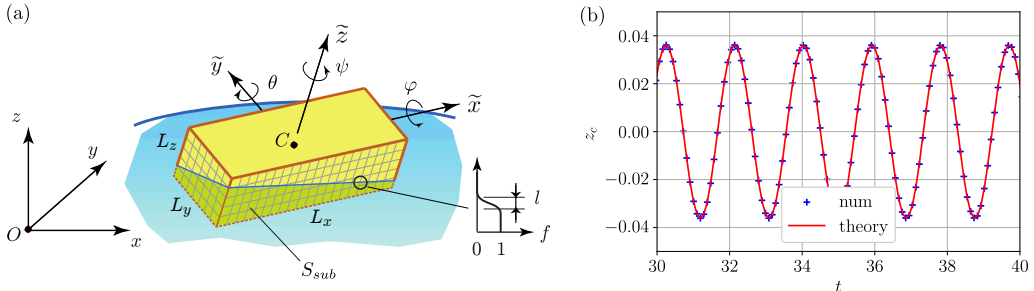


FIGURE 5. (a) Sketch of the floater and notations: laboratory frame  $(O, x, y, z)$ , moving floater frame  $(C, \tilde{x}, \tilde{y}, \tilde{z})$ , and Euler angles  $\theta$  (pitch),  $\phi$  (roll) and  $\psi$  (yaw). In the simulation, we numerically calculate the pressure force and torque on the submerged surface  $S_{sub}$  using rectangular meshes on each face and a mask function  $f$  that indicates whether the point on the face is submerged or not. (b) Free vertical oscillations of  $z_c$  at the bobbing frequency  $\sqrt{1/\beta\delta_z}$  in a numerical test-case without incoming wave

(iv) Steady streaming flows are negligible – The steady streaming flows is a nonlinear, mean flow correction of order  $O(\epsilon^2)$  that comes along with the linear wave. This mean flow can affect reorientation, but only if it is inhomogenous at the scale of the floater. Steady streaming flows typically vary spatially on the scale  $k^{-1}$ . Hence, with  $\delta = kL \ll 1$ , we expect a weak effect of streaming on the floater orientation.

(v) Wave scattering and wave emission are negligible (Froude-Krylov approximation) – In principle, floaters placed in an incoming wave act as obstacles and scatter this incoming wave. They can also move differentially with respect to the flow and hence emit waves. However, we can neglect these effects when the floater is small with respect to the wavelength and when differential motion is weak:

$$\delta = kL \ll 1 \quad , \quad \frac{\|\mathbf{u} - \mathbf{v}\|}{\|\mathbf{u}\|} \ll 1, \quad (3.1)$$

with  $\mathbf{u}$  the fluid velocity and  $\mathbf{v}$  floater velocity. We therefore assume that the floater only moves due to pressure forces and torques associated with the incoming wave.

The Froude-Krylov approximation is the most important assumption in our model. By neglecting the wave emission, we filter out radiative losses and added mass effects. As a result, free “bobbing” oscillations of the floater around the equilibrium position are not damped in our model. In practice, we avoid these free oscillations in our calculations using a particular initialisation strategy that will be detailed below. Another consequence of the absence of dissipation is that, as for an undamped pendulum, the equilibrium states must be either unstable or *marginally stable*. In our simulations, the yaw angle  $\psi$  will oscillate around the stable fixed point, rather than converging towards it as in the experiments.

### 3.2. Equations of motion

We derive equations of motion for a small parallelepiped floater drifting on a propagating gravity wave on infinitely deep water. We introduce a laboratory frame of reference  $(O, x, y, z)$ , with  $(\mathbf{e}_x, \mathbf{e}_y, \mathbf{e}_z)$  basis vectors (figure 5). By convention, the origin  $O$  is on the equilibrium fluid surface and the wave propagates along  $x$  and is  $y$ -invariant.

We use as incoming gravity wave the classical, linear potential wave solution on infinitely deep water

$$\zeta = a \sin(kx - \omega t), \quad \begin{cases} u_x = a\omega e^{kz} \sin(kx - \omega t) \\ u_z = -a\omega e^{kz} \cos(kx - \omega t) \end{cases}, \quad p = p_0 - \rho g z + \rho g a e^{kz} \sin(kx - \omega t). \quad (3.2)$$



Here  $\zeta$  is the surface elevation,  $u_x, u_z, p$  the velocity components and pressure,  $p_0$  the atmospheric pressure, and  $\omega = \sqrt{gk}$ . In the following, we non-dimensionalise space, time, velocity and pressure using the scales

$$[\mathbf{r}] = k^{-1} \quad , \quad [t] = (gk)^{-1/2} \quad , \quad [\mathbf{u}] = g^{1/2}k^{-1/2} \quad , \quad [p] = \rho g k^{-1}. \quad (3.3)$$

In this unit system, Eqs. (3.2) become

$$\zeta = \epsilon \sin(x - t), \quad \begin{cases} u_x = \epsilon e^z \sin(x - t) \\ u_z = -\epsilon e^z \cos(x - t) \end{cases}, \quad p = p_0 - z + \epsilon e^z \sin(x - t), \quad (3.4)$$

and the wave slope  $\epsilon = ka \ll 1$  is the only remaining parameter. In line with the Froude-Krylov assumption, we ignore the flow and pressure corrections caused by differential motion of the floater: only the incoming wave affects the floater motion in this model.

The floater is a rectangular parallelepiped with non-dimensional density  $\beta$ , non-dimensional length, width and height  $(\delta_x, \delta_y, \delta_z) = (kL_x, kL_y, kL_z)$ , and we assume that  $\delta_{x,y,z} \ll 1$ . We introduce a material frame  $(C, \tilde{x}, \tilde{y}, \tilde{z})$  co-moving with the floater, with  $C$  at the center of mass and the unit vectors  $(\tilde{\mathbf{e}}_x(t), \tilde{\mathbf{e}}_y(t), \tilde{\mathbf{e}}_z(t))$  aligned with the long, medium and short axes (figure 5). The instantaneous position of the floater is determined by the 3 coordinates  $x_c(t), y_c(t), z_c(t)$ , with

$$\mathbf{r}_c(t) = \mathbf{OC}(t) = x_c(t)\mathbf{e}_x + y_c(t)\mathbf{e}_y + z_c(t)\mathbf{e}_z, \quad (3.5)$$

and its orientation by the three Euler angles of roll  $\varphi(t)$ , pitch  $\theta(t)$  and yaw  $\psi(t)$ . These Euler angles define the transform that links the laboratory frame to the floater frame, and in our angle convention (see Appendix A) we have

$$\begin{bmatrix} \mathbf{e}_x \\ \mathbf{e}_y \\ \mathbf{e}_z \end{bmatrix} = \underbrace{\begin{bmatrix} c_\psi c_\theta & (c_\psi s_\theta s_\varphi - s_\psi c_\varphi) & (c_\psi s_\theta c_\varphi + s_\psi s_\varphi) \\ s_\psi c_\theta & (s_\psi s_\theta s_\varphi + c_\psi c_\varphi) & (s_\psi s_\theta c_\varphi - c_\psi s_\varphi) \\ -s_\theta & c_\theta s_\varphi & c_\theta c_\varphi \end{bmatrix}}_{R^T} \begin{bmatrix} \tilde{\mathbf{e}}_x \\ \tilde{\mathbf{e}}_y \\ \tilde{\mathbf{e}}_z \end{bmatrix}. \quad (3.6a)$$

Here and further we denote in short  $c_\psi = \cos \psi$ ,  $s_\psi = \sin \psi$  and similar for the other angles. This transform is easily inverted because  $R$  is an orthogonal matrix  $R^{-1} = R^T$ . Components of a vector  $\mathbf{A}$  and the coordinates of the laboratory and floater frame are also connected by this matrix,

$$\begin{bmatrix} A_x \\ A_y \\ A_z \end{bmatrix} = R^T \begin{bmatrix} \tilde{A}_x \\ \tilde{A}_y \\ \tilde{A}_z \end{bmatrix}, \quad \begin{bmatrix} x - x_c \\ y - y_c \\ z - z_c \end{bmatrix} = R^T \begin{bmatrix} \tilde{x} \\ \tilde{y} \\ \tilde{z} \end{bmatrix}. \quad (3.6b)$$

By definition, the floater moves as a solid. This means that an arbitrary point  $\mathbf{r}$  of the floater has velocity

$$\mathbf{v} = \mathbf{v}_c(t) + \boldsymbol{\Omega}(t) \times (\mathbf{r} - \mathbf{r}_c(t)), \quad (3.7)$$

with  $\mathbf{v}_c(t) = \dot{\mathbf{r}}_c(t)$  the translation velocity of the center of mass and  $\boldsymbol{\Omega}(t)$  the instantaneous rotation velocity. We decompose  $\mathbf{v}_c(t)$  in the lab-frame and  $\boldsymbol{\Omega}(t)$  in the floater frame and kinematically link these components to the derivatives of the coordinate functions by the relations

$$\begin{bmatrix} \dot{x}_c \\ \dot{y}_c \\ \dot{z}_c \end{bmatrix} = \begin{bmatrix} v_{c,x} \\ v_{c,y} \\ v_{c,z} \end{bmatrix}, \quad \begin{bmatrix} \dot{\varphi} \\ \dot{\theta} \\ \dot{\psi} \end{bmatrix} = \begin{bmatrix} 1 & \sin \varphi \tan \theta & \cos \varphi \tan \theta \\ 0 & \cos \varphi & -\sin \varphi \\ 0 & \frac{\sin \varphi}{\cos \theta} & \frac{\cos \varphi}{\cos \theta} \end{bmatrix} \begin{bmatrix} \tilde{\Omega}_x \\ \tilde{\Omega}_y \\ \tilde{\Omega}_z \end{bmatrix}. \quad (3.8)$$

The formula for the angles is non-trivial and depends on the convention used to define the angles (details given in Appendix A).

We now define the floater dynamics. From Newton's law and the angular momentum theorem for the floater, we have

$$m\dot{\mathbf{v}}_c = \mathbf{F} , \quad \frac{d}{dt} (\mathbf{I} \cdot \boldsymbol{\Omega}) = \mathbf{K}, \quad (3.9)$$

with  $m = \beta\delta_x\delta_y\delta_z$  the non-dimensional mass of the floater and  $\mathbf{I}$  the non-dimensional inertia tensor. The principal moments of inertia of the rectangular parallelepiped are

$$\tilde{I}_{xx} = \frac{m(\delta_y^2 + \delta_z^2)}{12}, \quad \tilde{I}_{yy} = \frac{m(\delta_z^2 + \delta_x^2)}{12}, \quad \tilde{I}_{zz} = \frac{m(\delta_x^2 + \delta_y^2)}{12}. \quad (3.10)$$

In our model, the floater is subject to gravity and to pressure forces and torques, given in non-dimensional form by

$$\mathbf{F} = \int_{S_{sub}} (p - p_0) d\mathbf{S} - m\mathbf{e}_z, \quad \mathbf{K} = \int_{S_{sub}} (\mathbf{r} - \mathbf{r}_c) \times (p - p_0) d\mathbf{S}, \quad (3.11)$$

with  $d\mathbf{S}$  orientated towards the floater, and  $S_{sub}$  the (time-dependent) submerged surface of the floater. In the Froude-Krylov approximation, the pressure  $p$  is that of equation (3.4) which contains a hydrostatic part and a dynamical part associated with the purely hydrodynamic, incoming wave (pressure corrections due to scattered and emitted waves are ignored in this model).

The previous surface integral formulation is used in the numerical simulations, but in the theory, we have found it easier to use an alternative, equivalent formulation of  $\mathbf{F}$  and  $\mathbf{K}$  in terms of volume integrals over the submerged volume  $V_{sub}$ . In equation (3.11), we can replace  $d\mathbf{S} = -d\mathbf{S}_{ext}$  so that the surface element is pointing from the floater towards the fluid. Using then the divergence theorem and the fact that  $\partial_t \mathbf{u} + \mathbf{e}_z = -\nabla p$  for the incoming linear wave we obtain the alternative formula

$$\mathbf{F} = \int_{V_{sub}} \mathbf{a} dV + \left( \int_{V_{sub}} dV - m \right) \mathbf{e}_z \quad (3.12a)$$

$$\mathbf{K} = \int_{V_{sub}} (\mathbf{r} - \mathbf{r}_c) \times \mathbf{a} dV + \int_{V_{sub}} (\mathbf{r} - \mathbf{r}_c) \times \mathbf{e}_z dV, \quad (3.12b)$$

with  $\mathbf{a} = \partial_t \mathbf{u}$  the local fluid acceleration. These formulas show better the leading Archimedes balance that defines the floater equilibrium in absence of waves ( $\mathbf{a} = 0$ ). Notice also that with  $a_y = 0$  for the incoming  $y$ -invariant wave, we also have  $F_y = 0$ : in this model, floaters will never be displaced along  $y$  and hence  $y_c$  remains constant.

We decompose Newton's law in the laboratory frame and the angular momentum equation in the floater frame. Using the fact that the material frame rotates along with the floater, i.e. that  $\dot{\tilde{\mathbf{e}}}_i(t) = \boldsymbol{\Omega}(t) \times \tilde{\mathbf{e}}_i(t)$ , we obtain

$$\begin{bmatrix} m\dot{v}_{x,c} \\ m\dot{v}_{y,c} \\ m\dot{v}_{z,c} \end{bmatrix} = \begin{bmatrix} F_x \\ F_y \\ F_z \end{bmatrix}, \quad \begin{bmatrix} \tilde{I}_{xx}\dot{\tilde{\Omega}}_x \\ \tilde{I}_{yy}\dot{\tilde{\Omega}}_y \\ \tilde{I}_{zz}\dot{\tilde{\Omega}}_z \end{bmatrix} = \begin{bmatrix} \tilde{K}_x + (\tilde{I}_{yy} - \tilde{I}_{zz})\tilde{\Omega}_y\tilde{\Omega}_z \\ \tilde{K}_y + (\tilde{I}_{zz} - \tilde{I}_{xx})\tilde{\Omega}_z\tilde{\Omega}_x \\ \tilde{K}_z + (\tilde{I}_{xx} - \tilde{I}_{yy})\tilde{\Omega}_x\tilde{\Omega}_y \end{bmatrix}. \quad (3.13)$$

We recognise the Euler equations for the rotation speed. Equations (3.13) combined with the kinematic relations (3.8) define a first order system of 12 differential equations. If we provide an initial state for the floater position and speed, we can numerically integrate this system forward in time.

In the absence of waves,  $\epsilon = 0$ , we expect the floaters to be in equilibrium, with  $\mathbf{F} = 0$

and  $\mathbf{K} = 0$ . Due to symmetry of the floater, we expect the Archimedes torque to vanish for a perfectly leveled, flat floater. From the Archimedes force balance, we can calculate the equilibrium submersion depth as  $\bar{h} = \beta\delta_z$ . The floater center  $C$  is exactly  $\delta_z/2$  above the bottom face of the floater. Hence, at equilibrium, we have floater coordinates

$$\bar{x}_c, \bar{y}_c, \bar{\psi} \text{ arbitrary} \quad , \quad \bar{z}_c = \left(\frac{1}{2} - \beta\right)\delta_z \quad , \quad \bar{\theta} = \bar{\varphi} = 0. \quad (3.14)$$

Here and further, we use bars to denote equilibrium positions.

### 3.3. Numerical simulations

To obtain a numerical solution to the specified equations of motion, we use the standard Runge-Kutta 4th order explicit numerical scheme. The numerical calculation of the surface integrals (3.11) that define  $\mathbf{F}$  and  $\mathbf{K}$  is non-trivial because the submerged surface  $S_{sub}$  varies in time. We use the following procedure to compute these integrals (see sketch of figure 5). On each of the six faces of the floater surface, we define two-dimensional rectangular meshes that contain  $\tilde{x}, \tilde{y}, \tilde{z}$  coordinates on those faces. To evaluate the force components  $F_x, F_y, F_z$  at a given time  $t$ , we use a loop that visits all six faces. On each face, we then first calculate the lab-frame  $(x, y, z)$  coordinates of the points on that face, using the coordinate transform (3.6b) and the present position  $x_c(t), y_c(t), z_c(t), \varphi(t), \theta(t), \psi(t)$ . With these lab-frame coordinates, we can then evaluate the pressure  $(p - p_0)$  on that face using (3.4). To handle the fact that the faces can be totally, partially or not submerged, we introduce an indicator function  $f = (1 + \tanh((\zeta(x, t) - z)/l))/2$ , with  $l$  a length over which the interface is smoothed. This function is equal to 1 in the liquid and 0 in the air and hence, the product  $(p - p_0)f$  is only non-zero on the submerged points of that face. Using a two-dimensional quadrature rule and the numerical values of  $(p - p_0)f$  on the face, we can then compute the surface integral on that face. Each face gives a local contribution to the force in the direction of the local inward normal  $d\mathbf{S}$ , so after having visited all 6 faces, we obtain the components  $\tilde{F}_x, \tilde{F}_y, \tilde{F}_z$  in the floater frame. Using the transform (3.6a) we then finally obtain the force components  $F_x, F_y, F_z$  in the lab frame. The torque components  $\tilde{K}_x, \tilde{K}_y, \tilde{K}_z$  are calculated in the same way.

We have done several static and dynamical tests in the absence of waves ( $\epsilon = 0$ ). In the static tests, we validated the calculation of  $\mathbf{F}$  and  $\mathbf{K}$  on floaters that were submerged and rotated to positions for which we could easily compute the force and torque analytically. In the dynamical tests, we used the code to reproduce sustained free oscillations of the floaters. When we release the floater slightly off an equilibrium position (3.14), we expect free ‘‘bobbing’’ oscillations in the vertical  $z_c$  or angular  $\theta, \varphi$  coordinates, of non-dimensional frequencies (Falnes & Kurniawan 2020)

$$\omega_z = \sqrt{\frac{1}{\beta\delta_z}}, \quad \omega_\theta = \sqrt{\frac{1}{\beta\delta_z} \left( \frac{\delta_x^2 + 6\beta(\beta - 1)\delta_z^2}{\delta_x^2 + \delta_z^2} \right)}, \quad \omega_\varphi = \sqrt{\frac{1}{\beta\delta_z} \left( \frac{\delta_y^2 + 6\beta(\beta - 1)\delta_z^2}{\delta_y^2 + \delta_z^2} \right)}. \quad (3.15)$$

Figure 5(b) shows an example of timeseries for free vertical oscillations in  $z_c$ , for a floater with  $\beta = 0.5$  released slightly above its equilibrium position  $z_c = 0$ . As illustrated in the figure, the expected oscillatory motion  $z_c = A \cos(\omega_z t)$  is accurately reproduced by our code.

The free oscillations in  $z_c, \theta, \varphi$  are useful to test the code but do not reflect the behavior of the floaters in our experiment. Restricting to floaters much smaller than the wavelength,  $\delta \ll 1$ , implies that the bobbing frequencies (3.15) are much larger than

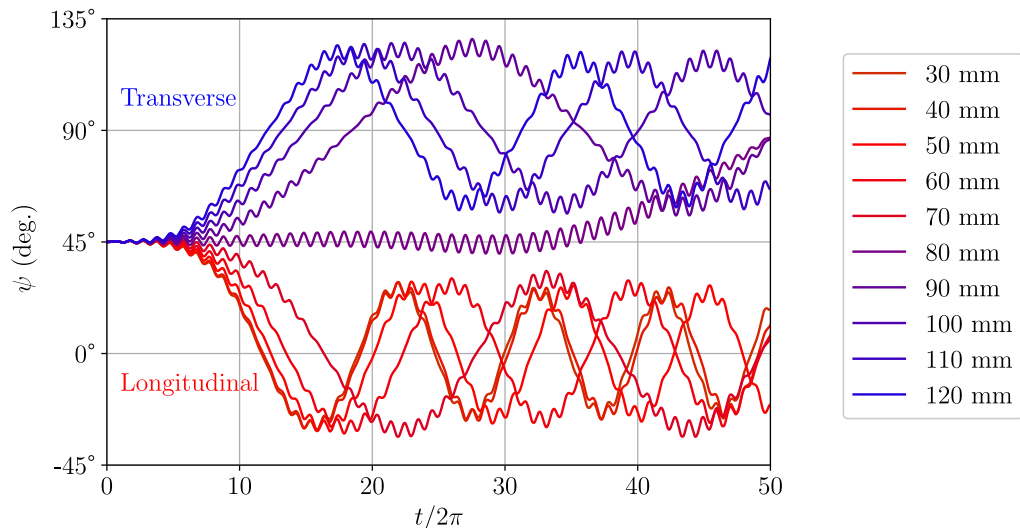


FIGURE 6. Time series for yaw angle for numerically simulated floaters with  $\beta = 0.44$ ,  $L_y = 10$  mm,  $L_z = 5$  mm and  $L_x$  varying from 30 to 120 mm. The incoming wave has wavelength  $\lambda = 0.29$  m and  $\epsilon = ka = 0.16$ , as in the experiments of figure 2. The L-T transition occurs near  $L_{xc} \approx 75$  mm, in good agreement with the experiments.

the incoming wave frequency ( $\omega = 1$  in non-dimensional units). Accordingly, such fast bobbing oscillations are never resonant, and are expected to be rapidly damped in the experiments, either by viscous friction or radiation loss. Since no damping is included in the simulations, we need to minimize these parasitic bobbing excitations. We use for this the following strategy: At time  $t = 0$ , we place the floater at its equilibrium position (3.14), and gradually ramp up the wave amplitude in time, by replacing  $\epsilon$  by  $\epsilon(1 - \exp(-t/T))$  in the definition of pressure and surface height (3.4). Practice shows that with  $T = 15 \times 2\pi$ , we can keep the fast bobbing oscillations of the floater motion at low amplitude while capturing the slow dynamics induced by the wave motion.

We now consider numerical solutions for the floater motion in presence of an incoming wave. In figure 6, we show time series of the yaw angle  $\psi(t)$ , for the same experimental conditions used in figure 2: floater size  $L_y = 10$  mm,  $L_z = 5$  mm and  $L_x$  varying from 30 to 120 mm, density ratio  $\beta = 0.44$ , wavelength  $\lambda = 0.29$  m and wave steepness  $\epsilon = ka = 0.16$ , initial yaw angle  $\psi_0 = 45^\circ$ . After a transient of typically 15 wave periods given by the ramp in the wave amplitude, the yaw angle  $\psi$  shows fast oscillations (of period  $2\pi$ ), that corresponds to the back and forth motion of the floaters, superimposed to slow oscillations around either the longitudinal position  $\psi = 0^\circ$  for short floaters or the transverse position  $\psi = 90^\circ$  for long floaters. The fast oscillations were not visible in figure 2(a) where the yaw angle measurement was synchronised at the wave frequency. The slow oscillations reflect the marginal stability of the fixed points in this dissipationless model. Apart from these differences, the numerical curves show a L-T transition somewhere in between  $L_x = 70$  mm and 80 mm, in excellent agreement with the experimental transition estimated at  $L_{xc} = 75$  mm for this set of floaters.

We have repeated the simulations for more than 500 floaters, with parameters varied in broad ranges and even slightly beyond the  $\epsilon, \delta \ll 1$  limit for which our model is designed:  $\beta \in [0.03, 0.97]$ ,  $\delta_x \in [0.004, 5.43]$ ,  $\delta_y \in [0.01, 0.36]$ ,  $\delta_z \in [0.007, 0.29]$ ,  $\epsilon \in [0.01, 0.33]$ . We summarize the preferential floater orientation in figure 7 using the same representation ( $F, \epsilon$ ) as in the experiments (Fig. 3). The L-T transition is clearly located at  $F_c = 60$

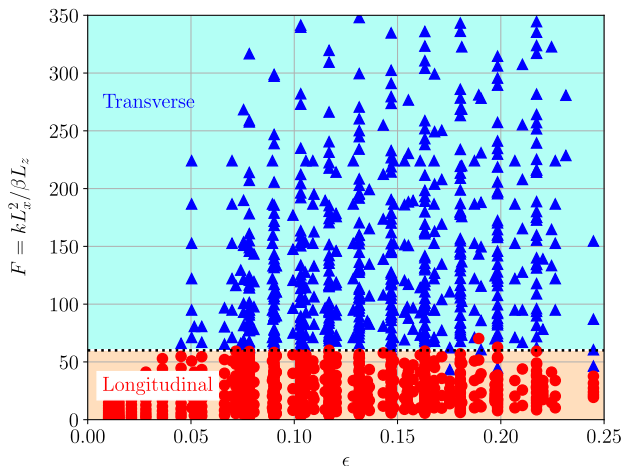


FIGURE 7. Preferential state of orientation in the  $(F, \epsilon)$  plane according to the numerical simulations. More than 500 numerical simulations have been performed for varying  $\beta, \delta_x, \delta_y, \delta_z, \epsilon$ , showing an excellent agreement with the theoretical prediction  $F_c = 60$ .

with no dependence in  $\epsilon$ , in excellent agreement with the asymptotic theory developed in the next section.

#### 4. Asymptotic description of floater motion

The main objective of this section is to use asymptotic theory to derive the nonlinear evolution equation (1.1) for the slow motion of the yaw angle  $\psi$  in the limit of  $\epsilon, \delta \ll 1$ , and to prove that the criterion (1.2) describes the L-T transition.

Let us start by specifying how the floater motion is decomposed in this theory. Without wave,  $\epsilon = 0$ , the floater is in its equilibrium position (3.14). With a low amplitude wave,  $\epsilon \ll 1$ , deviations from equilibrium can be parametrized as

$$\begin{cases} x_c = \bar{x}_c(\tau) + x'_c(t) + O(\epsilon^2) \\ y_c = \bar{y}_c \\ z_c = \bar{z}_c + z'_c(t) + O(\epsilon^2) \end{cases}, \quad \begin{cases} \theta = 0 + \theta'(t) + O(\epsilon^2) \\ \varphi = 0 + \varphi'(t) + O(\epsilon^2) \\ \psi = \bar{\psi}(\tau) + \psi'(t) + O(\epsilon^2) \end{cases} \quad (4.1)$$

Next to "mean" parts (bars) that are of order  $O(1)$ , we find smaller  $O(\epsilon)$  "oscillations" that vary on the rapid time-scale  $t$  of the wave (primes). We also admit that  $\bar{x}_c, \bar{\psi}$  can vary on a long time-scale  $\tau = t/\epsilon$ . The coordinate  $\bar{y}_c$  needs no further consideration as it remains constant in this Froude-Krylov model. In the calculation, we will first find the  $O(\epsilon)$  deviations  $x'_c(t), z'_c(t), \varphi'(t), \theta'(t), \psi'(t)$ , that carry the harmonic, linear response of the floater to the incoming wave. With this we can compute the second order,  $O(\epsilon^2)$  torque that defines the evolution equations of the yaw angle  $\bar{\psi}(\tau)$ .

The fact that roll and pitch angles  $\varphi, \theta$  always remain close to 0 allows to simplify (linearize) all the dependencies on these angles:  $s_\theta \approx \theta' + O(\epsilon^3), c_\theta \approx 1 + O(\epsilon^2), s_\varphi \approx \varphi' + O(\epsilon^3), c_\varphi \approx 1 + O(\epsilon^2)$ . The transform formula (3.6) then reduces to

$$\begin{bmatrix} \mathbf{e}_x \\ \mathbf{e}_y \\ \mathbf{e}_z \end{bmatrix} = \underbrace{\begin{bmatrix} c_\psi & -s_\psi & (c_\psi \theta' + s_\psi \varphi') \\ s_\psi & c_\psi & (s_\psi \theta' - c_\psi \varphi') \\ -\theta' & \varphi' & 1 \end{bmatrix}}_{\mathcal{R}^T} \begin{bmatrix} \tilde{\mathbf{e}}_x \\ \tilde{\mathbf{e}}_y \\ \tilde{\mathbf{e}}_z \end{bmatrix} + O(\epsilon^2) \quad (4.2)$$

and similar for the transform formula for vector components and coordinates in both

frames [see equation (3.6b)]. Up to  $O(\epsilon^2)$ , we can define the inverse transforms with the transposed matrix  $\mathcal{R}$ .

Let us now write a preliminary version of the evolution equations that determine these variables. For the first order deviations  $x'_c, z'_c, \varphi', \theta'$  we have

$$m\ddot{x}'_c = F'_x \quad , \quad m\ddot{z}'_c = F'_z \quad , \quad \tilde{I}_{xx}\ddot{\varphi}' = \tilde{K}'_x \quad , \quad \tilde{I}_{yy}\ddot{\theta}' = \tilde{K}'_y \quad (4.3)$$

The forces  $F'_x, F'_y$  and torques  $\tilde{K}'_x, \tilde{K}'_z$  contain the linearized,  $O(\epsilon)$  part of the total force and torque, and we explain below how they are calculated in practice. The evolution equation for the yaw angle  $\psi$  needs to be defined at order  $O(\epsilon^2)$  and this requires some attention. With small  $\theta, \varphi$ , we have  $s_\varphi \approx \varphi'$ ,  $\tilde{\Omega}_x \approx \dot{\varphi}'$  and  $\tilde{\Omega}_y \approx \dot{\theta}'$  at  $O(\epsilon)$ . From Eqs. (3.8) and (3.13) we then get that the equations

$$\dot{\psi} = \tilde{\Omega}_z + \varphi' \dot{\theta}' + O(\epsilon^3) \quad , \quad \tilde{I}_{zz}\dot{\tilde{\Omega}}_z = \tilde{K}_z + (\tilde{I}_{xx} - \tilde{I}_{yy})\dot{\varphi}'\dot{\theta}' \quad (4.4)$$

define the order  $O(\epsilon^2)$  description of yaw angle. These equations contain many different terms and so the description of the second order motion of the yaw angle seems rather complex. We remark the following simplification. Using the transform (4.2), the fact that  $\tilde{K}_x = \tilde{K}'_x + O(\epsilon^2)$ ,  $\tilde{K}_y = \tilde{K}'_y + O(\epsilon^2)$  and the evolution equations (4.3), we can rewrite the torque component  $\tilde{K}_z$  as

$$K_z = -\theta' \tilde{K}_x + \varphi' \tilde{K}_y + \tilde{K}_z \quad \Rightarrow \quad \tilde{K}_z = K_z + \tilde{I}_{xx}\dot{\varphi}'\dot{\theta}' - \tilde{I}_{yy}\dot{\varphi}'\dot{\theta}' \quad (4.5)$$

If we inject this expression of  $\tilde{K}_z$  into the second equation of (4.4) and use the first one to eliminate  $\tilde{\Omega}_z = \dot{\psi} - \varphi' \dot{\theta}'$ , we obtain the following equation for  $\psi$ :

$$\tilde{I}_{zz}\ddot{\psi} = K_z + \underbrace{\frac{d}{dt} \left( \tilde{I}_{xx}\dot{\varphi}'\dot{\theta}' - \tilde{I}_{yy}\dot{\varphi}'\dot{\theta}' + \tilde{I}_{zz}\dot{\varphi}'\dot{\theta}' \right)}_{\text{second order harmonics} \sim e^{\pm i2t}} + O(\epsilon^3) \quad (4.6)$$

In the right hand side, we find  $K_z$ , the vertical torque component in the lab-frame, next to a term  $d/dt(\dots)$  that is a time-derivative of  $O(\epsilon^2)$  products. In the evolution equation, this term can only produce harmonics with frequency  $\pm 2$ , but *no terms that are stationary*. As a consequence, this group of terms cannot create mean motion in  $\bar{\psi}$ . Of order  $O(\epsilon^2)$ , this term  $d/dt(\dots)$  will also have no effect on the  $O(\epsilon)$  rapid motion of  $\psi'$ . In summary, this just means that we can derive the equations for the yaw angle variables  $\bar{\psi}$  and  $\psi'$  from the balance  $\tilde{I}_{zz}\ddot{\psi} \approx K_z$  and this is a very significant simplification with respect to what we initially had in (4.4).

To separate the rapid from the slow motion, we still need to split the torque  $K_z$  into a rapidly varying  $O(\epsilon)$  fluctuating part and slowly varying  $O(\epsilon^2)$  mean part. We denote this as

$$K_z = \bar{K}_z + K'_z + O(\epsilon^3) \quad (4.7)$$

The part  $K'_z$  is of order  $O(\epsilon)$  and oscillates on the time-scale of the wave. The part  $\bar{K}_z$  is of order  $O(\epsilon^2)$  and is stationary on the rapid time-scale of the wave. Calculating this torque up to second order is the main difficulty in the asymptotic theory, but once we have it, the equations of motion for the yaw angle variables are as simple as

$$\tilde{I}_{zz}\ddot{\psi}' = K'_z \quad , \quad \tilde{I}_{zz}\ddot{\bar{\psi}} = \bar{K}_z \quad (4.8)$$

A preliminary version of the necessary evolution equations has now been specified, but we still need to calculate the force and torque components  $F'_x, F'_z, \tilde{K}'_x, \tilde{K}'_y, K'_z, \bar{K}_z$  analytically. We start from the volume formulation (3.12) of  $\mathbf{F}$  and  $\mathbf{K}$ . Analytical evaluation of these volume integrals is not simple for several reasons: (i) the submerged

volume  $V_{sub}$ , is continuously changing in time and this motion needs to be parametrised in floater frame coordinates  $(\tilde{x}, \tilde{y}, \tilde{z})$ , (ii) integrands are easily expressed in lab-frame coordinates  $(x, y, z)$ , but need to be expressed in floater frame coordinates. Both problems can be handled by making use of the assumption that the floater is small with respect to the wavelength. This allows to Taylor expand fields near the floater and in practice, to calculate the integrals.

Let us first explain how we handle problem (i), how we parametrise the volume integrals. In all calculations, we use

$$\int_{V_{sub}} \dots dV = \int_{-\delta_x/2}^{\delta_x/2} \int_{-\delta_y/2}^{\delta_y/2} \int_{-\delta_z/2}^{\tilde{\zeta}(\tilde{x}, \tilde{y}, t)} \dots d\tilde{x} d\tilde{y} d\tilde{z}. \quad (4.9)$$

We introduce here a new function,  $\tilde{\zeta}(\tilde{x}, \tilde{y}, t)$ , that defines the height of the water surface as seen in the floater frame. This way of calculating the integral implicitly supposes that the top face of the floater is never partially submerged ( $\tilde{\zeta} < \delta_z/2$ ) and that the bottom face is always totally submerged ( $\tilde{\zeta} > -\delta_z/2$ ) through the motion. This is a sensible approximation for low  $\epsilon$  and intermediate values of  $\beta$ . When  $\beta$  gets too close to 0 (very light floaters) or 1 (equal density floaters) we expect some discrepancies. Considering that the floater is supposed small with respect to the wavelength, we now construct  $\tilde{\zeta}(\tilde{x}, \tilde{y}, t)$  as a polynomial approximation, locally adapted near the floater. We start by Taylor expanding the surface elevation in the lab-frame  $\zeta(x, t)$  around  $x_c$ ,

$$\zeta(x, t) = \zeta_c + (x - x_c)\partial_x\zeta_c + \frac{(x - x_c)^2}{2}\partial_{xx}^2\zeta_c + \frac{(x - x_c)^3}{6}\partial_{xxx}^3\zeta_c + \dots \quad (4.10)$$

The index  $_c$  is used to express that the field is evaluated at the center of the floater  $C$ , e.g.  $\zeta_c = \zeta(x_c, t) = \epsilon \sin(x_c - t)$ ,  $\partial_x\zeta_c = \partial_x\zeta|_{x=x_c} = \epsilon \cos(x_c - t)$ , etc. We inject this Taylor expansion in the equation  $z = \zeta(x, t)$  that defines the free surface and we replace both  $z \approx z_c + (-\theta'\tilde{x} + \varphi'\tilde{y} + \tilde{z})$  and  $x - x_c \approx c_\psi\tilde{x} - s_\psi\tilde{y} + O(\epsilon)$ , the leading order parts of the coordinate transform formula (4.2). Reorganising this equation into  $\tilde{z} = \tilde{\zeta}(\tilde{x}, \tilde{y}, t)$  allows to identify

$$\begin{aligned} \tilde{\zeta}(\tilde{x}, \tilde{y}, t) = & \underbrace{-\bar{z}_c}_{O(\delta)} + \underbrace{-z'_c + \zeta_c}_{O(\epsilon)} + \underbrace{(\theta' + c_\psi\partial_x\zeta_c)\tilde{x} + (-\varphi' - s_\psi\partial_x\zeta_c)\tilde{y}}_{O(\epsilon\delta)} \\ & + \underbrace{\frac{1}{2}(c_\psi\tilde{x} - s_\psi\tilde{y})^2\partial_{xx}^2\zeta_c}_{O(\epsilon\delta^2)} + \underbrace{\frac{1}{6}(c_\psi\tilde{x} - s_\psi\tilde{y})^3\partial_{xxx}^3\zeta_c}_{O(\epsilon\delta^3)} + O(\epsilon^2, \epsilon\delta^4) \end{aligned} \quad (4.11)$$

For clarity, we group the terms that have same order of magnitude in terms of powers of  $\delta$  and  $\epsilon$ . We do not always need all the terms in this expansion but at some moments we do. With the function  $\tilde{\zeta}(\tilde{x}, \tilde{y}, t)$  known, we can split the integration over the submerged volume  $V_{sub}$  in two parts:

$$\int_{V_{sub}} \dots dV = \underbrace{\int_{-\delta_x/2}^{\delta_x/2} \int_{-\delta_y/2}^{\delta_y/2} \int_{-\delta_z/2}^{-\bar{z}_c} \dots d\tilde{x} d\tilde{y} d\tilde{z}}_{\int_{V_{sub}^{(0)}} \dots dV = O(\delta^3)} + \underbrace{\int_{-\delta_x/2}^{\delta_x/2} \int_{-\delta_y/2}^{\delta_y/2} \int_{-\bar{z}_c}^{\tilde{\zeta}} \dots d\tilde{x} d\tilde{y} d\tilde{z}}_{\int_{V_{sub}^{(1)}} \dots dV = O(\epsilon\delta^3)}. \quad (4.12)$$

The integral over  $V_{sub}^{(0)}$  covers the equilibrium submerged volume. The integral over  $V_{sub}^{(1)}$  covers the  $O(\epsilon)$  perturbation of submerged volume caused by the wave. In the theory, we

only need an  $O(\epsilon)$  approximation of this  $V_{sub}^{(1)}$  integral and then we can use

$$\int_{V_{sub}^{(1)}} f dV \approx \int_{-\delta_x/2}^{\delta_x/2} \int_{-\delta_y/2}^{\delta_y/2} f(\tilde{x}, \tilde{y}, -\bar{z}_c) \left( \tilde{\zeta}(\tilde{x}, \tilde{y}, t) + \bar{z}_c \right) d\tilde{x} d\tilde{y}. \quad (4.13)$$

as an approximation, where  $f$  is an arbitrary field.

Let us now explain how we handle problem (ii), i.e., how we express the integrands in the floater frame coordinates. In the force and torque formula (3.12), we find the fields

$$a_x = \partial_t u_x = -\epsilon e^z \cos(x - t) \quad , \quad a_z = \partial_t u_z = -\epsilon e^z \sin(x - t) \quad (4.14)$$

These fields depend on the lab-frame coordinates  $x, z$  but need to be expressed in terms of  $\tilde{x}, \tilde{y}, \tilde{z}$  variables if we want to compute the integrals analytically. Also here, the idea is to replace  $a_x, a_z$  with polynomial approximations, valid near the floater. Using Taylor series, we have

$$\begin{aligned} \mathbf{a} &= \mathbf{a}_c + (x - x_c) \partial_x \mathbf{a}_c + (z - z_c) \partial_z \mathbf{a}_c \\ &+ \frac{1}{2} (x - x_c)^2 \partial_{xx}^2 \mathbf{a}_c + \frac{1}{2} (z - z_c)^2 \partial_{zz}^2 \mathbf{a}_c + (x - x_c)(z - z_c) \partial_{xz}^2 \mathbf{a}_c + O(\epsilon \delta^3) \end{aligned} \quad (4.15)$$

Replacing  $x - x_c = c_\psi \tilde{x} - s_\psi \tilde{y} + (c_\psi \theta' + s_\psi \varphi') \tilde{z}$  and  $z - z_c = -\theta' \tilde{x} + \varphi' \tilde{y} + \tilde{z}$  from (4.2) we get

$$\mathbf{a} = \mathbf{a}^{(1)} + \mathbf{a}^{(2)} + O(\epsilon^3). \quad (4.16a)$$

There is an  $O(\epsilon)$  part

$$\begin{aligned} \mathbf{a}^{(1)} &= \underbrace{\mathbf{a}_c}_{O(\epsilon)} + \underbrace{(c_\psi \tilde{x} - s_\psi \tilde{y}) \partial_x \mathbf{a}_c + \tilde{z} \partial_z \mathbf{a}_c}_{O(\epsilon \delta)} \\ &+ \underbrace{\frac{1}{2} (c_\psi \tilde{x} - s_\psi \tilde{y})^2 \partial_{xx}^2 \mathbf{a}_c + \frac{\tilde{z}^2}{2} \partial_{zz}^2 \mathbf{a}_c + (c_\psi \tilde{x} - s_\psi \tilde{y}) \tilde{z} \partial_{xz}^2 \mathbf{a}_c}_{O(\epsilon \delta^2)} \end{aligned} \quad (4.16b)$$

and an  $O(\epsilon^2)$  part

$$\begin{aligned} \mathbf{a}^{(2)} &= \underbrace{(c_\psi \theta' + s_\psi \varphi') \tilde{z} \partial_x \mathbf{a}_c + (-\theta' \tilde{x} + \varphi' \tilde{y}) \partial_z \mathbf{a}_c}_{O(\epsilon^2 \delta)} \\ &+ \left[ (c_\psi \tilde{x} - s_\psi \tilde{y}) (c_\psi \theta' + s_\psi \varphi') \tilde{z} \partial_{xx}^2 \mathbf{a}_c + (-\theta' \tilde{x} + \varphi' \tilde{y}) \tilde{z} \partial_{zz}^2 \mathbf{a}_c \right. \\ &\quad \left. + [(c_\psi \tilde{x} - s_\psi \tilde{y}) (-\theta' \tilde{x} + \varphi' \tilde{y}) + (c_\psi \theta' + s_\psi \varphi') \tilde{z}^2] \partial_{xz}^2 \mathbf{a}_c \right]. \end{aligned} \quad (4.16c)$$

$O(\epsilon^2 \delta^2)$

This second order part  $\mathbf{a}^{(2)}$  is of no importance for the harmonic, linear response of the floater to the wave. However, it does contribute to the second order mean torque  $\bar{K}_z$ .

We now have explained all the mathematical tools that are needed to calculate the force and torque components. Using the notations of the previous paragraphs, we use the following formula to compute the  $O(\epsilon)$  fluctuating forces and torques that appear in the



equations of motion (4.3):

$$F'_x = \left( \int_{V_{sub}^{(0)}} a_x^{(1)} dV \right)_{(\bar{x}_c, \bar{z}_c, \bar{\psi})} \quad (4.17a)$$

$$F'_z = \left( \int_{V_{sub}^{(0)}} a_z^{(1)} dV + \int_{V_{sub}^{(1)}} dV \right)_{(\bar{x}_c, \bar{z}_c, \bar{\psi})} \quad (4.17b)$$

$$\tilde{K}'_x = \left( \int_{V_{sub}^{(0)}} (\tilde{y} a_z^{(1)} + s_\psi \tilde{z} a_x^{(1)} - \tilde{z} \varphi') dV + \int_{V_{sub}^{(1)}} \tilde{y} dV \right)_{(\bar{x}_c, \bar{z}_c, \bar{\psi})} \quad (4.17c)$$

$$\tilde{K}'_y = \left( \int_{V_{sub}^{(0)}} (-\tilde{x} a_z^{(1)} + c_\psi \tilde{z} a_x^{(1)} - \tilde{z} \theta') dV + \int_{V_{sub}^{(1)}} (-\tilde{x}) dV \right)_{(\bar{x}_c, \bar{z}_c, \bar{\psi})} \quad (4.17d)$$

To obtain the formula for these torque components, we have used  $\mathbf{r} - \mathbf{r}_c = \tilde{x} \tilde{\mathbf{e}}_x + \tilde{y} \tilde{\mathbf{e}}_y + \tilde{z} \tilde{\mathbf{e}}_z$  and the fact that  $\mathbf{a} = c_\psi a_x \tilde{\mathbf{e}}_x - s_\psi a_x \tilde{\mathbf{e}}_y + a_z \tilde{\mathbf{e}}_z + O(\epsilon^2)$  in the floater frame, according to the transform (4.2). In practice, the calculation of these integrals is not particularly difficult as we only have to integrate polynomials. The subscript  $(\bar{x}_c, \bar{z}_c, \bar{\psi})$  expresses that the formula, obtained after integration, needs to be evaluated at the equilibrium position  $x_c \approx \bar{x}_c$ ,  $z_c \approx \bar{z}_c$  and  $\psi \approx \bar{\psi}$ .

Remain the torque components  $\bar{K}_z$  and  $K'_z$  that need to be calculated up to respective orders  $O(\epsilon^2)$  and  $O(\epsilon)$ . Using the definition of  $K_z$  and the coordinate transform formula for  $y - y_c$ , we have

$$K_z = - \int_{V_{sub}} (y - y_c) a_x dV = - \int_{V_{sub}} (s_\psi \tilde{x} + c_\psi \tilde{y} + (s_\psi \theta' - c_\psi \varphi') \tilde{z}) a_x dV + O(\epsilon^3).$$

Using the previous notations, we separate this torque in two parts  $K_z = K_z^{(1)} + K_z^{(2)} + O(\epsilon^3)$  of respective orders  $O(\epsilon)$  and  $O(\epsilon^2)$ . We have

$$K_z^{(1)} = - \int_{V_{sub}^{(0)}} (s_\psi \tilde{x} + c_\psi \tilde{y}) a_x^{(1)} dV \quad (4.18a)$$

$$K_z^{(2)} = - \int_{V_{sub}^{(0)}} (s_\psi \theta' - c_\psi \varphi') \tilde{z} a_x^{(1)} dV - \int_{V_{sub}^{(0)}} (s_\psi \tilde{x} + c_\psi \tilde{y}) a_x^{(2)} dV - \int_{V_{sub}^{(1)}} (s_\psi \tilde{x} + c_\psi \tilde{y}) a_x^{(1)} dV. \quad (4.18b)$$

These torques  $K_z^{(1)}$  and  $K_z^{(2)}$  are not yet the torques  $K'_z$  and  $\bar{K}_z$  that enter the evolution equations of  $\psi'$  and  $\bar{\psi}$ . The fluctuating torque is just

$$K'_z = \left( K_z^{(1)} \right)_{(\bar{x}_c, \bar{z}_c, \bar{\psi})} \quad (4.19)$$

which is equation (4.18a) evaluated at the equilibrium position. The  $O(\epsilon^2)$  mean torque  $\bar{K}_z$  is more subtle and has two parts

$$\bar{K}_z = \overline{\left( K_z^{(1)} \right)_{(\bar{x}_c + x'_c, \bar{z}_c + z'_c, \bar{\psi} + \psi')}} + \overline{\left( K_z^{(2)} \right)_{(\bar{x}_c, \bar{z}_c, \bar{\psi})}} \quad (4.20)$$

The bars in the right hand side denote a time-average. The second term is just the time-average of  $K_z^{(2)}$  evaluated at the equilibrium position. The first term is a "drift"-like contribution that can be understood in the same way as we understand the Stokes drift phenomenon (Stokes 1847). As the floater moves along with the wave, goes through its first order motion, it explores regions of slightly higher and lower velocity. On average,

this can result in a net displacement (Stokes drift) and here, for our spatially extended floaters, it also results in a weak  $O(\epsilon^2)$  mean torque. In practice, we calculate this "drift"-like torque by using a Taylor series around the equilibrium position  $(\bar{x}_c, \bar{z}_c, \bar{\psi})$ . Up to order  $O(\epsilon^2)$  we may use

$$\bar{K}_z \approx \underbrace{\overline{(K_z^{(1)})}_{(\bar{x}_c, \bar{z}_c, \bar{\psi})}}_0 + \overline{\left( x'_c \frac{\partial K_z^{(1)}}{\partial x_c} + z'_c \frac{\partial K_z^{(1)}}{\partial z_c} + \psi' \frac{\partial K_z^{(1)}}{\partial \psi} \right)}_{(\bar{x}_c, \bar{z}_c, \bar{\psi})} + \overline{(K_z^{(2)})}_{(\bar{x}_c, \bar{z}_c, \bar{\psi})} \quad (4.21)$$

The first term vanishes because we are taking the time-average of  $K'_z$  that is by constructing a quantity that fluctuates on the time-scale of the wave. The second group carries the mean effective torque and requires the first order motion  $x'_c, z'_c, \psi'$ .

The integrals defining  $F'_x, F'_z, \tilde{K}'_x, \tilde{K}'_y, K'_z, \bar{K}_z$  or now clearly defined but one question remains. We still need to estimate to which order in  $\delta$  we must push all the Taylor series that we use to approximate  $\tilde{\zeta}$  and the fields  $\mathbf{a}^{(1)}, \mathbf{a}^{(2)}$  in the integrands. Considering the equations of motion (4.3) and (4.8), and the fact that  $m = O(\delta^3)$  and  $\mathbf{I} = O(\delta^5)$ , we deduce that we needed to calculate

$$\begin{aligned} F'_x, F'_z & \text{ up to order } O(\epsilon\delta^4) \\ \tilde{K}'_x, \tilde{K}'_y, K'_z & \text{ up to order } O(\epsilon\delta^6) \\ \bar{K}_z & \text{ up to order } O(\epsilon^2\delta^6). \end{aligned} \quad (4.22)$$

The idea is that this should give access to the leading,  $O(\epsilon)$  description of  $x'_c, z'_c, \varphi', \theta', \psi'$ ,  $O(\epsilon^2)$  description of  $\bar{\psi}$ , but also to floater shape-related corrections of respective orders  $O(\epsilon\delta)$  and  $O(\epsilon^2\delta)$ . In the limit  $\delta \ll 1$ , these shape-corrections seem much smaller but this is without considering that these  $O(\epsilon\delta)$  and  $O(\epsilon^2\delta)$  terms are actually taking the form of  $O(\epsilon\delta_x^2/\beta\delta_z)$  and  $O(\epsilon^2\delta_x^2/\beta\delta_z)$  terms. For strongly elongated floater, we can easily have

$$\frac{\delta_x^2}{\beta\delta_z} \sim 1 \quad (4.23)$$

and in that case, the shape related corrections may become as large or even larger than the so-called leading order terms. This is precisely what happens at the L-T transition and a theoretical pain in the neck: we really need to push the calculation of the forces and torques to the orders of (4.22), otherwise we will miss the terms that stabilise the transverse equilibrium. This, on the contrary is too much and results in very long, unpractical formula. In our view, the best way, in between calculating no shape-related corrections and all shape related correction, is to add an extra assumption. In the experiment, all the floaters are flat and this means that

$$\delta_x, \delta_y \gg \delta_z \quad (4.24)$$

is a fair assumption. By exploiting this information in the calculation of the forces and torques we can ignore (i) all  $O(\delta_z)$  terms with respect to  $O(1)$  terms, (ii) all  $O(\delta_z^2)$  terms with respect to  $O(\delta_x^2, \delta_y^2)$  terms. This greatly simplifies the theory and produces a physically relevant result. We can in fact, even further simplify the model by taking into account that our floaters are also very elongated  $\delta_x \gg \delta_y$  in our experiments. This will be done at the end, but in our calculation, we have found it useful to keep  $\delta_x, \delta_y$  at similar magnitude as it produces more symmetrical formula that allow supplementary checks. For now, we continue our presentation with the flat floater assumption (4.24).

Once  $F'_x, F'_z, \tilde{K}'_x, \tilde{K}'_y, K'_z$  are found, we immediately have the differential equations for the first order motion  $x'_c, z'_c, \varphi', \theta', \psi'$ . Solving these differential equations is rather trivial

and yields the harmonic response

$$x'_c \approx \epsilon \cos(\bar{x}_c - t) \quad (4.25a)$$

$$z'_c \approx \epsilon \left( 1 - \frac{1}{24} (\bar{c}_\psi^2 \delta_x^2 + \bar{s}_\psi^2 \delta_y^2) \right) \sin(\bar{x}_c - t). \quad (4.25b)$$

$$\varphi' \approx -\epsilon \bar{s}_\psi \left( 1 - \left( \bar{s}_\psi^2 \frac{\delta_y^2}{40} + \bar{c}_\psi^2 \frac{\delta_x^2}{24} \right) \right) \cos(\bar{x}_c - t) \quad (4.25c)$$

$$\theta' \approx -\epsilon \bar{c}_\psi \left( 1 - \left( \bar{c}_\psi^2 \frac{\delta_x^2}{40} + \bar{s}_\psi^2 \frac{\delta_y^2}{24} \right) \right) \cos(\bar{x}_c - t) \quad (4.25d)$$

$$\psi' \approx \epsilon \left( \frac{\delta_x^2 - \delta_y^2}{\delta_x^2 + \delta_y^2} \right) \bar{s}_\psi \bar{c}_\psi \sin(\bar{x}_c - t), \quad (4.25e)$$

Let us interpret these equations. At leading  $O(\epsilon)$  order, we find in  $x'_c$  and  $z'_c$  that the floater oscillates around its mean position, just as a material particle on the wave-surface would do. Although this is less trivial to see, the leading  $O(\epsilon)$  expressions for the angles  $\varphi'$ ,  $\theta'$  are such that the flat floater rotates so to align with the local wave slope (imagine the rotation of a surfboard on a long wavelength wave that passes). The yaw angle  $\psi'$  rocks back and forth around the mean value and thus the more for sufficiently elongated floaters with  $\delta_x \gg \delta_y$  and for  $\bar{\psi}$  close to  $45^\circ$ . Next the leading  $O(\epsilon)$  terms, we also have some smaller, shape-related corrections of order  $O(\epsilon \delta_x^2, \epsilon \delta_y^2)$  in the  $z'_c, \varphi', \theta'$  variables. These corrections may seem utterly small but we really can not ignore them. Physically, they are due the fact that the water surface is not perfectly flat at the scale of the floater. This waterline curvature induces small modification in the buoyancy force that affect the force  $F'_z$  and the torques  $\tilde{K}_x, \tilde{K}_y$ . In particular the  $O(\epsilon \delta_x^2)$  correction in  $z'_c$  is essential in this problem: without it, we just cannot explain why long floaters prefer the transverse equilibrium. In section 5 we provide a more physical understanding of what this correction actually captures.

With the first order motion specified, we can continue to next order. The evaluation of the second order mean torque  $\bar{K}_z$  is a difficult and technical part in this calculation (some elements are provided in Appendix B). More important is that for flat floaters with  $\delta_x, \delta_y \gg \delta_z$ , we obtain the following nonlinear equation of motion for the slowly varying yaw angle

$$\ddot{\bar{\psi}} = \epsilon^2 \left[ \bar{s}_\psi \bar{c}_\psi^3 \left( -\frac{(\delta_x^2 - \delta_y^2) \delta_x^2}{(\delta_x^2 + \delta_y^2)^2} + \frac{\frac{\delta_x^4}{60} - \frac{\delta_x^2 \delta_y^2}{48}}{\beta \delta_z (\delta_x^2 + \delta_y^2)} \right) - \bar{s}_\psi^3 \bar{c}_\psi \left( -\frac{(\delta_y^2 - \delta_x^2) \delta_x^2}{(\delta_x^2 + \delta_y^2)^2} + \frac{\frac{\delta_y^4}{60} - \frac{\delta_x^2 \delta_y^2}{48}}{\beta \delta_z (\delta_x^2 + \delta_y^2)} \right) \right] \quad (4.26)$$

We can separate a common factor  $\bar{s}_\psi \bar{c}_\psi$  in the right hand side and because of this term, we know that longitudinal ( $\bar{\psi} = 0^\circ$ ) and transverse ( $\bar{\psi} = 90^\circ$ ) positions are equilibria. We can also verify how this equation incorporates a fundamental symmetry: if we exchange  $\delta_x \leftrightarrow \delta_y$  and rotate the angle  $\bar{\psi} \rightarrow \bar{\psi} + \pi/2$ , then the rectangular floater is in the same physical state. When  $\delta_x = \delta_y$ , a new fixed point emerges at  $\bar{\psi} = 45^\circ$ , but the idea of preferential orientation then loses its interest.

The equation for the slow evolution of yaw angle can be used to discuss the stability of the L and T states. However, this discussion becomes even simpler with the extra assumption of very elongated floaters:  $\delta_x \gg \delta_y \gg \delta_z$ . Ignoring all  $O(\delta_y^2)$  terms with respect to  $O(\delta_x^2)$  terms, we can simplify (4.26) further to find the equation of motion

(1.2) already mentioned in the introduction

$$\delta_x \gg \delta_y \gg \delta_z : \quad \ddot{\bar{\psi}} = -\epsilon^2 \bar{s}_\psi \bar{c}_\psi^3 \left( 1 - \underbrace{\frac{\delta_x^2}{60\beta\delta_z}}_{F/F_c} \right). \quad (4.27)$$

This confirms that the non-dimensional number

$$F = \frac{\delta_x^2}{\beta\delta_z} = \frac{kL_x^2}{\beta L_z} \quad (4.28)$$

is the control parameter that sets the preferential state of orientation. When  $F = F_c = 60$ , the right hand side changes change sign and this is indicative of a global change in stability. To see this better, we rewrite the equation in conservative form

$$\ddot{\bar{\psi}} = -\frac{dV(\bar{\psi})}{d\bar{\psi}}, \quad V(\bar{\psi}) = \frac{\epsilon^2}{4} \left( -1 + \frac{F}{F_c} \right) \bar{c}_\psi^4. \quad (4.29)$$

This equation tells us that the slow motion of the yaw angle is analogous to that of a particle in a potential well  $V(\bar{\psi}) \sim \cos^4 \bar{\psi}$ . For short floaters with  $F < F_c = 60$ , the longitudinal position of  $\bar{\psi} = 0^\circ$  is the minimum of the potential and hence the stable state. For long floaters with  $F > F_c$ , the situation flips and the transverse equilibrium,  $\bar{\psi} = 90^\circ$  becomes the potential minimum and the stable state, in excellent agreement with the experiments (figure 3) and the numerical simulations (figure 7).

## 5. Simplified model and physical interpretation

The asymptotic approach already provided some physical insights, but the calculation of the second order torque  $\bar{K}_z$  is so technical that much of the simpler physics remains hidden. In this section, we show how to find the evolution equation for  $\bar{\psi}$  much more rapidly, by bringing in some physical ideas earlier on in the calculation.

We recall that both the rapid and slow motion of yaw angle  $\psi$  are controlled by the torque component

$$K_z = \mathbf{e}_z \cdot \int_{V_{sub}} (\mathbf{r} - \mathbf{r}_c) \times \mathbf{a} \, dV = - \int_{V_{sub}} (y - y_c) a_x \, dV, \quad (5.1)$$

with  $a_x = -\epsilon e^z \cos(x-t)$ . Evaluating this integral is the main difficulty in the theory and there are numerous contributions that all need careful consideration (see Appendix B). We have seen at the end of the previous section that the limit of strongly elongated floaters  $\delta_x \gg \delta_y \gg \delta_z$  is clearly adapted to capture the preferential orientation phenomenon, so let us exploit this information directly. If the floater is indeed thin (along  $\tilde{z}$ ) and not wide (along  $\tilde{y}$ ), we can simply ignore the  $\tilde{y}$  and  $\tilde{z}$  variations in this torque integral and simplify it to

$$K_z \approx - \int_{-\delta_x/2}^{+\delta_x/2} (y - y_c) a_x \delta_y \underbrace{\left( \tilde{\zeta} + \frac{\delta_z}{2} \right)}_{\tilde{h}(\tilde{x},t)} d\tilde{x}. \quad (5.2)$$

For this formula to make sense, we must express  $(y - y_c)a_x$  in terms of floater frame coordinates and ignore the  $\tilde{y}$  and  $\tilde{z}$  variations. We also need to find the local submersion depth  $\tilde{h}(\tilde{x}, t) = \tilde{\zeta} + (\delta_z/2)$  along the long  $\tilde{x}$ -axis of the floater. To get this done, we use a simplified coordinate transform. From (4.2) and ignoring all dependencies along  $\tilde{y}$  and  $\tilde{z}$ , we find that

$$x \approx x_c + c_\psi \tilde{x}, \quad y \approx y_c + s_\psi \tilde{x}, \quad z \approx z_c - \theta' \tilde{x} \quad (5.3)$$

along the long axis of the floater. The lever arm is then  $y - y_c \approx s_\psi \tilde{x}$ . The dependence of the field  $a_x$  on  $\tilde{x}$  can be found by injecting this coordinate transform in the theoretical expression. Then, making use of a Taylor expansion we get

$$\begin{aligned} a_x &\approx -\epsilon e^{z_c - \theta' \tilde{x}} \cos(x_c + c_\psi \tilde{x} - t) \\ &\approx -\epsilon (1 + z_c - \theta' \tilde{x}) (\cos(x_c - t) - c_\psi \tilde{x} \sin(x_c - t)) + \dots \end{aligned} \quad (5.4)$$

up to  $O(\epsilon^2)$ . To find the local submersion depth  $\tilde{h}(\tilde{x}, t)$ , we ignore the  $\tilde{y}$ -dependencies in the general definition of  $\tilde{\zeta}$  in (4.11). We also use the fact that  $-\bar{z}_c + (\delta_z/2) = \beta L_z = \bar{h}$  is the equilibrium submersion depth. In this way, we find that the local submersion depth  $\tilde{h}(\tilde{x}, t)$  along the floater long axis is

$$\tilde{h}(\tilde{x}, t) \approx \bar{h} + (-z'_c + \epsilon \sin(x_c - t)) + (\theta' + \epsilon c_\psi \cos(x_c - t)) \tilde{x} - \frac{\epsilon}{2} c_\psi^2 \tilde{x}^2 \sin(x_c - t). \quad (5.5)$$

The wave surface at the scale of the floater is here approximated by a second order polynomial and this is sufficient in this simplified model (we do not need the third derivate terms). In this expression, we need to insert the first order motion  $z'_c$  and  $\theta'$ . We already know the first order motion from the asymptotic theory, but let us show how we can alternatively find this motion using some simpler physical arguments. In the pressure force and torque, the buoyancy terms are the largest ones, much larger than the dynamical pressure terms. Hence, we estimate that the floater is moving in such a way that it keeps its submersed volume nearly constant in time. This requires

$$\frac{1}{\delta_x} \int_{-\delta_x/2}^{+\delta_x/2} \tilde{h}(\tilde{x}, t) d\tilde{x} \approx \bar{h} \quad (5.6)$$

Evaluating the integral using the expression (5.5), we get the result

$$z'_c \approx \epsilon \sin(x_c - t) \left( 1 - \frac{\delta_x^2}{24} c_\psi^2 \right). \quad (5.7)$$

This indeed corresponds to the expression of  $z'_c$  that we have obtained from a more formal treatment of the equations of motion, in the limit  $\delta_x \gg \delta_y$ , see equation (4.25b). Interestingly, we also recover the shape-related  $O(\epsilon \delta_x^2)$  correction that is quite crucial in the model. To explain the angular motion  $\theta'$ , we can use a similar physical argument. Due to buoyancy, the floater will rotate so as to align with the local surface slope. The local normal on the wave surface is  $\mathbf{n} \approx \nabla(z - \zeta(x, t))|_{x=x_c} = \mathbf{e}_z - \epsilon \cos(x_c - t) \mathbf{e}_x$  and then needs to be orthogonal to the long axis  $\tilde{\mathbf{e}}_x \approx c_\psi \mathbf{e}_x + s_\psi \mathbf{e}_y - \theta' \mathbf{e}_z$ . Hence, we get

$$\mathbf{n} \cdot \tilde{\mathbf{e}}_x \approx 0 \quad \Rightarrow \quad \theta' = -\epsilon c_\psi \cos(x_c - t). \quad (5.8)$$

This approximation is sufficient, the extra  $O(\epsilon \delta_x^2)$  correction in  $\theta'$  of (4.25d) is in fact not so important. Replacing these expressions of  $z'_c$  and  $\theta'$  into (5.5), we find the following approximation for the local shape of the waterline at the floater position

$$\tilde{h}(\tilde{x}, t) \approx \bar{h} + \epsilon c_\psi^2 \left( \frac{\delta_x^2}{24} - \frac{\tilde{x}^2}{2} \right) \sin(x_c - t). \quad (5.9)$$

This result can be interpreted as follows: the waterline as seen from the floater center always takes the shape of a parabola, symmetrical around  $\tilde{x} = 0$ .

Combining all the elements together, we end up with the following simplified formula

for the mean yaw moment  $K_z$ :

$$K_z \approx - \int_{-\delta_x/2}^{+\delta_x/2} \underbrace{\tilde{x}s_\psi}_{\text{local lever arm}} \underbrace{(-\epsilon(1+z_c-\theta'\tilde{x})(\cos(x_c-t)-c_\psi\tilde{x}\sin(x_c-t)))}_{\text{local force density } f_x} \times \underbrace{\left(\bar{h} + \epsilon c_\psi^2 \left(\frac{\delta_x^2}{24} - \frac{\tilde{x}^2}{2}\right) \sin(x_c-t)\right)}_{\text{local submersion } \tilde{h}} \delta_y d\tilde{x}. \quad (5.10)$$

This integral contains all the physics that explains the preferential orientation. The torque  $K_z$  is the result of the local force density  $f_x$  that varies along the floater's long axis applied on the local level arm. This force density is weighted by the local submersion depth  $\tilde{h}$  and this effect is thus more important as the floater is longer. We evaluate this integral up to  $O(\epsilon^2)$  and write the evolution equation  $\tilde{I}_{zz}\dot{\psi} = K_z$ . Approximating  $\tilde{I}_{zz} \approx m\delta_x^2/12$  for our elongated floater, we find

$$\ddot{\psi} \approx -\epsilon(1+z_c)s_\psi c_\psi \sin(x_c-t) - \epsilon\theta' s_\psi \cos(x_c-t) + \frac{\epsilon^2\delta_x^2}{30\beta\delta_z} s_\psi c_\psi^3 \sin^2(x_c-t). \quad (5.11)$$

We now inject in this equation the decomposition  $x_c = \bar{x}_c + x'_c$  and  $z_c = \bar{z}_c + z'_c$ . In the first,  $O(\epsilon)$  term of (5.11), we use a Taylor expansion:

$$\begin{aligned} & -\epsilon(1+\bar{z}_c+z'_c)s_\psi c_\psi \sin(\bar{x}_c+x'_c-t) \\ & = -\epsilon(1+\bar{z}_c)s_\psi c_\psi \sin(\bar{x}_c-t) - \epsilon z'_c s_\psi c_\psi \sin(\bar{x}_c-t) - \epsilon x'_c s_\psi c_\psi \cos(\bar{x}_c-t) + O(\epsilon^3). \end{aligned} \quad (5.12)$$

As the floater is thin, we can approximate  $\bar{z}_c \approx 0$ . The second and third terms of (5.11) are already of order  $O(\epsilon^2)$ , so there we can use  $\sin^2(x_c-t) \approx \sin^2(\bar{x}_c-t) + O(\epsilon)$  and  $\cos(x_c-t) \approx \cos(\bar{x}_c-t) + O(\epsilon)$ . We then replace the first order deviations by

$$x'_c \approx \epsilon \cos(\bar{x}_c-t) \quad , \quad z'_c \approx \epsilon \sin(\bar{x}_c-t) \quad , \quad \theta' = -\epsilon c_\psi \cos(\bar{x}_c-t). \quad (5.13)$$

The expression of  $x'_c$  can be found by integrating  $\dot{x}'_c = u_x|_{z=0}$ , which just means that, at lowest order, the floater translates as a fluid material particle on the surface. After these reductions, we obtain

$$\ddot{\psi} \approx -\epsilon s_\psi c_\psi \sin(\bar{x}_c-t) + \epsilon^2 s_\psi c_\psi \left(-1 + \frac{\delta_x^2}{30\beta\delta_z} c_\psi^2\right) \sin^2(\bar{x}_c-t) \quad (5.14)$$

as evolution equation for  $\psi$ . We now also inject the decomposition  $\psi = \bar{\psi} + \psi'$  and use a Taylor expansion to replace

$$s_\psi c_\psi = \bar{s}_\psi \bar{c}_\psi + \psi'(\bar{c}_\psi^2 - \bar{s}_\psi^2) + O(\epsilon^2). \quad (5.15)$$

This yields

$$\begin{aligned} \ddot{\bar{\psi}} + \ddot{\psi}' & \approx -\epsilon \bar{s}_\psi \bar{c}_\psi \sin(\bar{x}_c-t) \\ & -\epsilon(\bar{c}_\psi^2 - \bar{s}_\psi^2)\psi' \sin(\bar{x}_c-t) + \epsilon^2 \bar{s}_\psi \bar{c}_\psi \left(-1 + \frac{\delta_x^2}{30\beta\delta_z} \bar{c}_\psi^2\right) \sin^2(\bar{x}_c-t). \end{aligned} \quad (5.16)$$

At order  $O(\epsilon)$ , we identify the equation for the fast yaw angle excursion  $\ddot{\psi}' = -\epsilon \bar{s}_\psi \bar{c}_\psi \sin(\bar{x}_c-t)$ , that has the solution

$$\psi' \approx \epsilon \bar{s}_\psi \bar{c}_\psi \sin(\bar{x}_c-t). \quad (5.17)$$

This expression is identical to that of the asymptotic model (4.25e) in the limit  $\delta_x \gg$

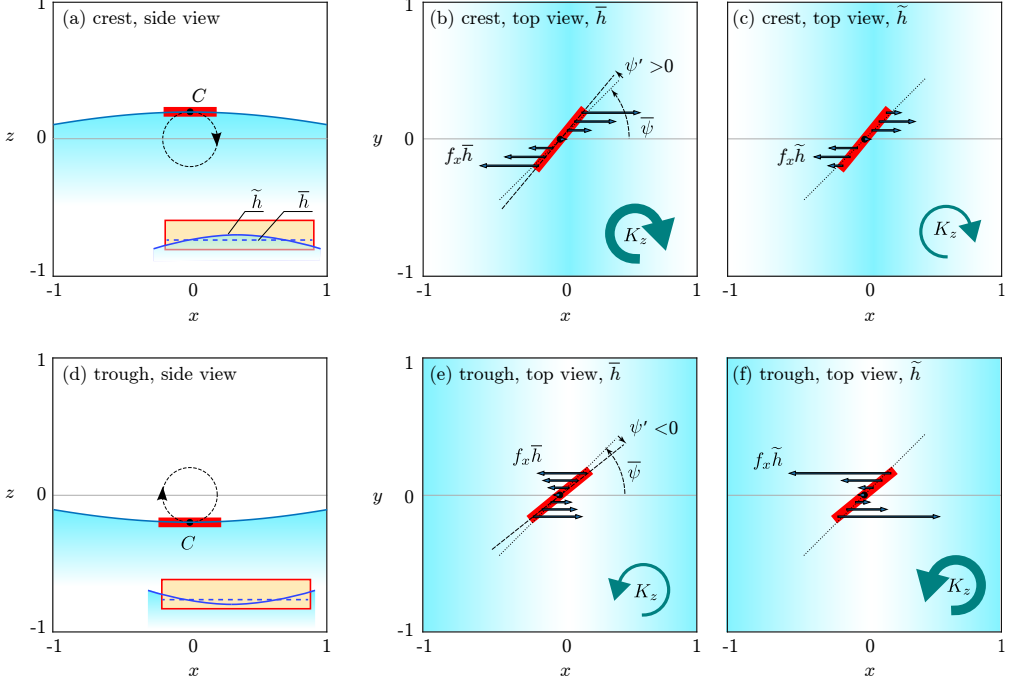


FIGURE 8. Position, orientation and force distribution on the floater in wave crests and troughs. Here  $\delta_x = 0.5$ ,  $\delta_z = 0.01$ ,  $\beta = 0.2$ ,  $\epsilon = 0.2$  and  $\bar{x}_c = 0$ ,  $\bar{\psi} = 45^\circ$ . (a,d) Side views on vertical  $x - z$  plane. The circle shows the trajectory of the center of mass. The inset figures suggest the instantaneous, parabolic shape of the waterline near the floater. (b,c,e,f) top views on  $x - y$  plane. The arrows show the instantaneous force distribution along the floater that creates the instantaneous torque  $K_z$ . In (b,e), without considering the variable submersion depth, using  $\bar{h}$ . In (c,f) taking into account the variable submersion  $\tilde{h}$ .

$\delta_y$ . Injecting this expression of  $\psi'$  back into the equation, we isolate the second order evolution equation for  $\bar{\psi}$  by averaging over time and find

$$\ddot{\bar{\psi}} \approx \epsilon^2 \bar{s}_\psi \bar{c}_\psi^3 \left( 1 - \underbrace{\frac{\delta_x^2}{60\beta\delta_z}}_{F/F_c} \right). \quad (5.18)$$

Hence, we have shown that the simplified model reproduces exactly the more formal asymptotic theory.

The main advantage of the simplified model is that it allows a better understanding of the physics that causes reorientation. Let us reconsider the torque  $K_z$  in (5.10), expressed as the product of the local force density  $f_x$  by the local level arm weighted by the local submersion depth  $\tilde{h}$ . The force density  $f_x$  is illustrated as vector arrows in figure 8, showing the floater at two times,  $t = \pi/2$  and  $t = 3\pi/2$  (wave crest and trough); animations are available as Supplementary Materials. The parameters are  $\beta = 0.2$ ,  $\delta_x = 0.5$ ,  $\delta_z = 0.01$  and  $\epsilon = 0.2$ , corresponding to a non-dimensional number  $F = \delta_x^2/\beta\delta_z = 125$ , larger than the critical value  $F_c = 60$ : this floater will prefer the transverse position at late times. In the second column [Figs. 8(b,e)], the force distribution is weighted by the equilibrium, spatially uniform submersion depth  $\bar{h}$ , whereas in the third column [Figs. 8(c,f)] it is weighted by the true, varying depth  $\tilde{h}$ .

Comparing both cases allows us to illustrate the main physical mechanisms at the origin of the longitudinal-transverse transition.

We first consider the case where the depth variation is ignored [Figs. 8(b,e)], an approximation acceptable for small floaters only. At the wave crest, the yaw angle is slightly larger than the mean value  $\bar{\psi}$  whereas at the trough, it is slightly smaller than  $\bar{\psi}$ . The lever arm,  $\tilde{x} \sin \psi$ , is therefore larger at the crest. We also see that the local force density  $f_x$  is slightly larger at the crest than at the trough. Both effects impact the instantaneous torque in the same way. At the crest, the floater will experience a negative (clockwise) torque  $K_z < 0$  that is slightly larger than the positive (counter-clockwise) torque  $K_z > 0$  in the troughs, explaining why the part  $-\tilde{x} \sin \psi f_x \bar{h}$  in the integrand of  $K_z$  is slowly pushing the floater towards the longitudinal position.

Figures 8(c,f) illustrates why including the varying submersion in the weighting of the force distribution changes this conclusion in the case of long floaters. We immediately see that there is clear influence of the variable submersion at the tips of the floater: the weighted force density  $f_x \tilde{h}$  is significantly changing in magnitude. As shown in Figs. 8(a,d), at the wave crest, the extremities of the floater are less submerged, whereas in the troughs, they are more submerged. This locally changing submersion implies that the instantaneous torque is significantly decreased at the tips of the floater when they are at crest and increased at the tips when the floater is in a trough. The result for this floater with  $F = 125 > F_c$  is that the positive (counter-clockwise) torque  $K_z > 0$  acting on the floater at the troughs is significantly larger than the negative torque at the crests, resulting in a slow rotation towards the transverse position.

It is finally interesting to note that the yaw angle motion of small floaters is analogous to that of the Kapitza pendulum, a pendulum with an oscillating anchor point (Kapitza 1951; Landau & Lifschitz 1960; Butikov 2001). For small floaters we have seen that the variation of the immersion depth can be ignored and in that case, we have the evolution equation

$$F \ll F_c : \ddot{\psi} \approx -\epsilon s_\psi c_\psi \sin(\bar{x}_c - t) - \epsilon^2 s_\psi c_\psi \sin^2(\bar{x}_c - t). \quad (5.19)$$

Using the fact that  $s_\psi c_\psi = (1/2) \sin 2\psi$  and changing notation  $2\psi = \alpha$ , we can rewrite this as

$$\ddot{\alpha} + \underbrace{\left( -\frac{\epsilon^2}{2} + \underbrace{\epsilon \sin(\bar{x}_c - t)}_{g'(t)} + O(\epsilon^2) \right)}_{\bar{g}} \sin \alpha \approx 0. \quad (5.20)$$

We recognize the equation of motion for the angle  $\alpha$  of a Kapitza pendulum, written in the frame of reference attached to the anchor point. The Kapitza pendulum, analogue to our floater, would be exposed to a weak  $O(\epsilon^2)$  downward external gravity  $\bar{g}$  and a larger  $O(\epsilon)$  oscillatory acceleration  $g(t)$  that is due to the motion of the anchor point. Using the same multiple time-scale techniques as we have previously used, we can find that this pendulum has two equilibria. The lower position  $\bar{\alpha} = 0^\circ$  is stable and the top position,  $\bar{\alpha} = 180^\circ$  is unstable. Owing to the relation  $\bar{\psi} = \bar{\alpha}/2$ , this result is entirely equivalent to saying that short floaters prefer longitudinal positions,  $\bar{\psi} = 0^\circ$ , and avoid transverse positions,  $\bar{\psi} = 90^\circ$ .

## 6. Mean yaw moment: comparison with the literature

We have formulated a theoretical model for the idealized, second order motion of the yaw angle, but in the existing literature, the focus is not so much on the slow yaw motion, but rather on the mean yaw moment  $\bar{K}_z$ . Several articles provide quantitative results for this mean yaw moment, either in the form of an explicit equation (equation (55)



in Newman (1967)) or in the form of figures that result from numerical computations (Newman 1967; Skejic & Faltinsen 2008; Chen 2007; Yasukawa *et al.* 2019). In this section, we compare the second order yaw moment that we have calculated from our Froude-Krylov model to some existing results, focusing on the limit  $\delta_x \gg \delta_y \gg \delta_z$  of a strongly elongated floater.

To allow comparison, let us start by writing the dimensional yaw moment according to our theory. By multiplying the right hand side of (1.1) with the dimensional moment of inertia  $\beta\rho L_x^3 L_y/12$  and  $\omega^2 = gk$ , we obtain

$$\bar{K}_z = \frac{1}{12}\rho g a^2 k^3 L_x^3 L_y \left( -\beta L_z + \frac{kL_x^2}{60} \right) \sin \bar{\psi} \cos^3 \bar{\psi}. \quad (6.1)$$

This formula only applies to parallelepiped floaters that are short with respect to the wavelength. As explained before, part of the torque (contribution  $-\beta L_z$  in the parentheses) favors a longitudinal floater position (head-seas). This torque clearly depends on how deep the floater is submerged as the draft of our floater is  $\bar{h} = \beta L_z$ . The other part of the torque (contribution  $+kL_x^2/60$  in the parentheses) favors a transverse floater position (beam-seas) and interestingly, it does not depend on the draft.

Newman (1967) derived an analytical formula [see his equation (55)] for the mean yaw moment on a slender floating structure with rectangular planform, such as our parallelepipeds. Written in our notations (wavenumber  $K \rightarrow k$ , width  $B \rightarrow L_y$ , length  $L \rightarrow L_x$ , angle of incidence  $\beta = -\bar{\psi}$ ), this mean yaw moment is

$$\bar{K}_z^{\text{Newman}} = \frac{1}{2}\rho g k a^2 L_x^2 L_y \sin \bar{\psi} j_1 \left( \frac{1}{2}kL_x \cos \bar{\psi} \right) j_2 \left( \frac{1}{2}kL_x \cos \bar{\psi} \right). \quad (6.2)$$

Here  $j_1$  and  $j_2$  are spherical Bessel functions. In this formula, diffraction and radiation are taken into account so it holds for any  $kL_x$ . In the limit of small floater length, we can replace the spherical Bessel functions with their small argument asymptotic expansions. From Abramowitz & Stegun (1948), equation (10.1.2), we have  $j_1(x)j_2(x) \approx x^3/45$  for small  $x$  (rather than  $x^3/3$  as written in Newman (1967)), so (6.2) reduces to

$$kL_x \cos \bar{\psi} \ll 1 : \bar{K}_z^{\text{Newman}} \approx \frac{1}{12}\rho g a^2 k^3 L_x^3 L_y \left( \frac{kL_x^2}{60} \right) \sin \bar{\psi} \cos^3 \bar{\psi}. \quad (6.3)$$

Interestingly, this equation contains exactly one term of our mean yaw moment (6.1), the one that favors the transverse position. The other term, related to the draft  $\bar{h} = \beta L_z$ , is absent, probably because Newman used a slender body approximation which may hold as long as  $kL_x^2/\bar{h} \gg 1$ . This missing term explains why Newman's formula does not predict a stable longitudinal position for short floaters. The fact that our asymptotic theory based on the Froude-Krylov assumption recovers the short floater limit of Newman's theory is somehow surprising: in our approach, we neglect wave diffraction and radiation, whereas the existence of a radiated wave is essential in Newman's far field theory. This suggests that the diffracted/radiated wave correction in the near field of small floaters does not contribute at leading order to the mean yaw moment acting on such small floaters.

In his *middle-field* formulation, Chen (2007) introduced a numerical approach to calculate first order motion and second order load on quite general floating structures. The potential field around the floating body is calculated using the boundary element method and includes diffracted and radiated waves. In one numerical application, Chen considers a very large floating platform, called FPSO (Floating Production Storage Offloading)-unit, that is close to a parallelepiped with dimensions  $L_x = 300$  m by  $L_y = 50$  m and submerged over  $\bar{h} = \beta L_z = 25$  m – huge compared to our centimeter scale parallelepiped floaters –, placed in waves with angle of incidence  $\bar{\psi} = -165^\circ$ .

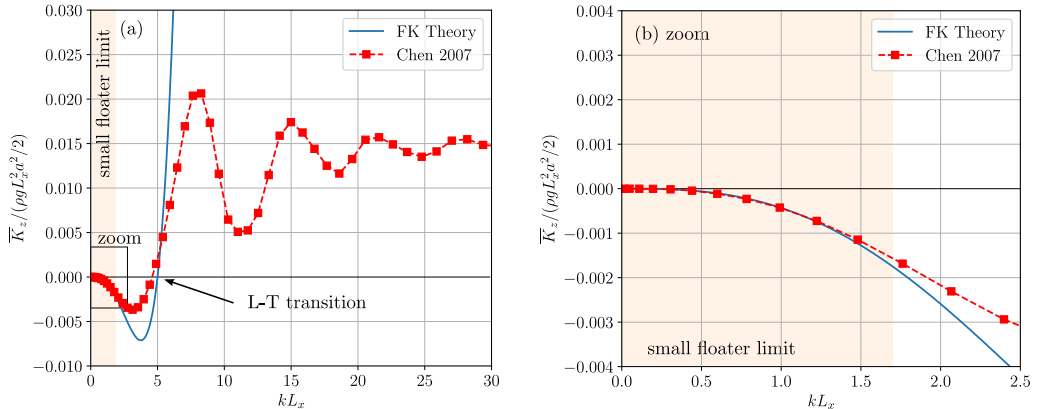


FIGURE 9. (a) Dimensionless mean yaw moment as a function of  $kL_x$ , and (b) zoom at small  $kL_x$ . Red squares: Data from the boundary element simulations of Chen (2007), computed for a 300-m long floating structure. Blue line: present Froude-Krylov theory (6.1), valid in the limit  $kL_x \leq 1$ , when diffraction and radiation is negligible. The longitudinal-transverse transition, where  $\bar{K}_z = 0$  (or  $F = F_c$ ), is approximately the same for both methods.

In common sea conditions, wavelengths are usually shorter than 300 m, so we expect diffraction and wave radiation corrections, ignored in our theory, to be important. In figure 9(a), we compare the mean yaw moment calculated by Chen’s BEM approach (red squares) and our Froude-Krylov theory (6.1) (blue line). As  $kL_x$  increases, the mean yaw moment calculated by Chen is first negative, before changing sign and oscillating at larger  $kL_x$ , a signature of diffraction and radiation effects. As emphasized by the zoom in figure 9(b), the  $-(kL_x)^4$  trend at small  $kL_x$  is very well reproduced by our theory. In spite of the strong departure of our formula from the simulation at larger  $kL_x$ , it reproduces surprisingly well the change of sign of  $\bar{K}_z$ , marking the longitudinal-transverse transition. Although this might be coincidental, this suggests that the criterium  $kL_x^2/\bar{h} \simeq 60$  for the transition still applies at moderate  $kL_x$ , even when diffraction and radiation effects are not negligible.

## 7. Conclusion

In this paper we have shown that the orientation of a small elongated floater drifting in a propagating gravity wave is governed by the non-dimensional number  $F = kL_x^2/\bar{h}$ , where  $\bar{h} = \beta L_z$  is the equilibrium submersion depth. Short and deeply immersed floaters align longitudinally, along with the direction of propagation, whereas long and weakly immersed floaters prefer to align transversely, along with the wave crests or troughs.

To model the preferential orientation of these drifting elongated floaters, we introduced a Froude-Krylov theory that assumes a linear potential incoming wave in infinitely deep water, ignoring viscous and capillary effects and all feedbacks of the floater on the wave. We numerically solved the equations of motion and demonstrated that this model contains the dominant physical ingredients that are needed to reproduce the preferential state of orientation. In the limit of small wave amplitude and small floaters,  $\epsilon, \delta \ll 1$ , we derived an asymptotic solution of the Froude-Krylov model. This classical and rather technical asymptotic method allows us to find the second order evolution equation (1.2) for the slow motion of the yaw angle, and places the L-T transition at  $F_c = 60$ , which is reasonably close to the experimental value  $F_c \simeq 45 \pm 10$ .

To gain deeper insight into the physics of the floater orientation, we have finally shown

that the same evolution equation (1.2) for the slow motion of the yaw angle can be found using a simpler approach in the limit of strongly elongated floaters. This allowed us to identify that the preferential orientation is the result of local gradients in flow magnitude that the floater experiences through its motion. Short floaters see little variation in submersion depth along their long axis and experience a mean torque that favors the longitudinal position. This mean torque arises from a phase correlation between the oscillating buoyancy force and the oscillating lever arm, a feature shared with the classical Kapitza pendulum. For longer floaters, the variation of the submersion along the floater has a strong effect on the instantaneous torque, that is significantly decreased in crest positions (the tips are less submerged) and increased in trough positions (the tips are more submerged). Since in the trough position, the instantaneous torque always pushes towards the transverse position, long floaters prefer to take transverse positions.

We have compared our mean yaw moment formula to previously published results. Compared to Newman's theory, we have identified an additional contribution to the mean yaw moment that varies linearly with the draft  $\bar{h}$ . The longitudinal-transverse transition for short floaters is due to this contribution, explaining why Newman's prediction, that slender structures are stable in beam-seas, does not apply for very short floaters. Comparing our Froude-Krylov theory to Chen's boundary element calculations applied to a large floating structure, we obtain an excellent agreement for the mean yaw moment in the small floater length/ wavelength limit, and a fair prediction for the longitudinal-transverse transition. Away from this limit, diffraction and radiation are no longer negligible and our simplified theory breaks down. It would be interesting to extend these comparisons to smaller floating structures such as sailing boats or small yachts.

We can finally draw some parallels between our work and recent studies in relation to the problem of plastic waste transport by waves. The effect of shape on the mean motion of non-spherical objects in wave flows has been investigated in several studies, but limited to fully submerged, neutrally buoyant ellipsoids (DiBenedetto *et al.* 2018; DiBenedetto & Ouellette 2018; DiBenedetto *et al.* 2019; Clark *et al.* 2020; DiBenedetto *et al.* 2022). A similar preferential orientation phenomenon is observed there too, but its physical origin is very different: it results from the pressure and viscous stress distribution on their surface (Jeffery 1922), while for floating elongated bodies it results from the non-uniform pressure forces and spatially varying submersion. This raises the question of the drift and preferential orientation of very small, millimeter scale, floating anisotropic particles, for which both viscous and buoyancy effects are expected.

## Acknowledgments

We are grateful to J. Andriamampianina, A. Eddi, M. Le Boulluec, L. Martin-Witkowski and M. Rabaud for fruitful discussions, and X. Chen for sharing his numerical data on the mean yaw moment. We thank A. Aubertin, L. Auffray, J. Amarni and R. Pidoux for experimental help.

## Appendix A. Kinematics of rotation

We detail in this Appendix the Euler angle convention used in this article, and find the kinematic relation that links  $\dot{\varphi}(t), \dot{\theta}(t), \dot{\psi}(t)$  to the components  $\tilde{\Omega}_x(t), \tilde{\Omega}_y(t), \tilde{\Omega}_z(t)$  of the instantaneous rotation vector in the floater frame.

The instantaneous orientation of the floater is defined with three Euler angles  $\theta(t)$  pitch,  $\varphi(t)$  roll and  $\psi(t)$  yaw. These angles relate to three successive rotations that bring the laboratory frame  $(\mathbf{e}_x, \mathbf{e}_y, \mathbf{e}_z)$  to the floater frame  $(\tilde{\mathbf{e}}_x(t), \tilde{\mathbf{e}}_y(t), \tilde{\mathbf{e}}_z(t))$ . Imagine looking

at the wave from above, from the  $\mathbf{e}_z$  axis. The yaw angle  $\psi(t)$  is the angle over which we need to rotate the laboratory frame to align the  $\mathbf{e}'_x$ -axis of a new frame, with the front of the floater. This defines a first intermediate frame  $(\mathbf{e}'_x, \mathbf{e}'_y, \mathbf{e}'_z)$  as

$$\begin{bmatrix} \mathbf{e}'_x \\ \mathbf{e}'_y \\ \mathbf{e}'_z \end{bmatrix} = \underbrace{\begin{bmatrix} \cos \psi & \sin \psi & 0 \\ -\sin \psi & \cos \psi & 0 \\ 0 & 0 & 1 \end{bmatrix}}_{R_\psi} \begin{bmatrix} \mathbf{e}_x \\ \mathbf{e}_y \\ \mathbf{e}_z \end{bmatrix}. \quad (\text{A } 1)$$

$R_\psi$  is a first rotation matrix. We now change our point of view and look at the floater from the side, from the  $\mathbf{e}'_y$  direction. The pitch angle  $\theta(t)$  is the angle over which we need to rotate the  $(\mathbf{e}'_x, \mathbf{e}'_y, \mathbf{e}'_z)$  frame to find a new  $\mathbf{e}''_x$  axis that aligns with the nose of the boat. Hence, we have a second intermediate frame  $(\mathbf{e}''_x, \mathbf{e}''_y, \mathbf{e}''_z)$  defined as

$$\begin{bmatrix} \mathbf{e}''_x \\ \mathbf{e}''_y \\ \mathbf{e}''_z \end{bmatrix} = \underbrace{\begin{bmatrix} \cos \theta & 0 & -\sin \theta \\ 0 & 1 & 0 \\ \sin \theta & 0 & \cos \theta \end{bmatrix}}_{R_\theta} \begin{bmatrix} \mathbf{e}'_x \\ \mathbf{e}'_y \\ \mathbf{e}'_z \end{bmatrix}. \quad (\text{A } 2)$$

$R_\theta$  is a second rotation matrix. In a third and final rotation, we imagine looking at the boat from the front, from the  $\mathbf{e}''_x$  direction. The roll angle  $\varphi(t)$ , rotates the  $(\mathbf{e}''_x, \mathbf{e}''_y, \mathbf{e}''_z)$  frame to the floater frame. Hence, we have

$$\begin{bmatrix} \tilde{\mathbf{e}}_x \\ \tilde{\mathbf{e}}_y \\ \tilde{\mathbf{e}}_z \end{bmatrix} = \underbrace{\begin{bmatrix} 1 & 0 & 0 \\ 0 & \cos \varphi & \sin \varphi \\ 0 & -\sin \varphi & \cos \varphi \end{bmatrix}}_{R_\varphi} \begin{bmatrix} \mathbf{e}''_x \\ \mathbf{e}''_y \\ \mathbf{e}''_z \end{bmatrix}, \quad (\text{A } 3)$$

and  $R_\varphi$  is a third rotation matrix. All combined and using the fact that the rotation matrices are orthogonal, we can explicit the passage from the laboratory frame to the floater frame as

$$\begin{bmatrix} \tilde{\mathbf{e}}_x \\ \tilde{\mathbf{e}}_y \\ \tilde{\mathbf{e}}_z \end{bmatrix} = \underbrace{R_\varphi R_\theta R_\psi}_R \begin{bmatrix} \mathbf{e}_x \\ \mathbf{e}_y \\ \mathbf{e}_z \end{bmatrix}, \quad \begin{bmatrix} \mathbf{e}_x \\ \mathbf{e}_y \\ \mathbf{e}_z \end{bmatrix} = \underbrace{R_\psi^T R_\theta^T R_\varphi^T}_{R^T} \begin{bmatrix} \tilde{\mathbf{e}}_x \\ \tilde{\mathbf{e}}_y \\ \tilde{\mathbf{e}}_z \end{bmatrix}. \quad (\text{A } 4)$$

Evaluating these matrix products explicitly we obtain formula (3.6a).

We now explain how to find (3.8) that links  $\dot{\psi}(t), \dot{\theta}(t), \dot{\varphi}(t)$  to  $\tilde{\Omega}_x(t), \tilde{\Omega}_y(t), \tilde{\Omega}_z(t)$ . The floater frame rotates at instantaneous speed  $\tilde{\Omega}(t)$  which can be expressed using the differential equation  $\dot{\tilde{\mathbf{e}}}_i(t) = \tilde{\Omega}(t) \times \tilde{\mathbf{e}}_i(t)$  for  $i = x, y, z$ . In other terms, we have

$$\frac{d}{dt} \begin{bmatrix} \tilde{\mathbf{e}}_x \\ \tilde{\mathbf{e}}_y \\ \tilde{\mathbf{e}}_z \end{bmatrix} = \underbrace{\begin{bmatrix} 0 & \tilde{\Omega}_z & -\tilde{\Omega}_y \\ -\tilde{\Omega}_z & 0 & \tilde{\Omega}_x \\ \tilde{\Omega}_y & -\tilde{\Omega}_x & 0 \end{bmatrix}}_M \begin{bmatrix} \tilde{\mathbf{e}}_x \\ \tilde{\mathbf{e}}_y \\ \tilde{\mathbf{e}}_z \end{bmatrix}. \quad (\text{A } 5)$$

Considering the transform (3.6a), we can also compute the time-derivative of the vectors of the floater frame by deriving the rotation matrix. We then have

$$\frac{d}{dt} \begin{bmatrix} \tilde{\mathbf{e}}_x \\ \tilde{\mathbf{e}}_y \\ \tilde{\mathbf{e}}_z \end{bmatrix} = \frac{d}{dt} (R_\varphi R_\theta R_\psi) \begin{bmatrix} \mathbf{e}_x \\ \mathbf{e}_y \\ \mathbf{e}_z \end{bmatrix} = \frac{d}{dt} (R_\varphi R_\theta R_\psi) (R_\psi^T R_\theta^T R_\varphi^T) \begin{bmatrix} \tilde{\mathbf{e}}_x \\ \tilde{\mathbf{e}}_y \\ \tilde{\mathbf{e}}_z \end{bmatrix}. \quad (\text{A } 6)$$

Comparing with (A 5) implies

$$\left( R'_\varphi R_\theta R_\psi \dot{\varphi} + R_\varphi R'_\theta R_\psi \dot{\theta} + R_\varphi R_\theta R'_\psi \dot{\psi} \right) R_\psi^T R_\theta^T R_\varphi^T = M. \quad (\text{A } 7)$$

We denote  $R'_\varphi = \partial_\varphi R_\phi$  and similar for the other matrices. Considering the orthogonality of the rotation matrices, this simplifies to  $R'_\varphi R_\phi^T \dot{\varphi} + R_\varphi R'_\theta R_\theta^T \dot{\theta} + R_\varphi R_\theta R'_\psi R_\psi^T R_\theta^T R_\phi^T \dot{\psi} = M$ . After evaluating all the matrix products, we then deduce that

$$\begin{bmatrix} \tilde{\Omega}_x \\ \tilde{\Omega}_y \\ \tilde{\Omega}_z \end{bmatrix} = \begin{bmatrix} 1 & 0 & -\sin \theta \\ 0 & \cos \varphi & \cos \theta \sin \varphi \\ 0 & -\sin \varphi & \cos \theta \cos \varphi \end{bmatrix} \begin{bmatrix} \dot{\varphi} \\ \dot{\theta} \\ \dot{\psi} \end{bmatrix} \quad (\text{A } 8)$$

Notice that this matrix is singular, when  $\theta = \pm\pi/2$ . In our applications, we do not encounter such large pitch angles. Hence, we can always invert this relation to find the system of equations (3.8).

## Appendix B. Extra details of the asymptotic calculation

The computation of  $F'_x, F'_z, \tilde{K}'_x, \tilde{K}'_y, K'_z$  and the simplifications due to use of the flat floater assumption yield the following differential equations for the first order motion

$$\ddot{x}'_c \approx -\epsilon \cos(\bar{x}_c - t) \quad (\text{B } 1a)$$

$$\ddot{z}'_c + \frac{1}{\beta\delta_z} z'_c \approx \epsilon \left[ \frac{1}{\beta\delta_z} - 1 - \frac{1}{24\beta\delta_z} (\bar{c}_\psi^2 \delta_x^2 + \bar{s}_\psi^2 \delta_y^2) \right] \sin(\bar{x}_c - t) \quad (\text{B } 1b)$$

$$\ddot{\varphi}' + \frac{1}{\beta\delta_z} \varphi' \approx -\epsilon \bar{s}_\psi \left[ \frac{1}{\beta\delta_z} - 1 - \frac{1}{\beta\delta_z} \left( \bar{s}_\psi^2 \frac{\delta_y^2}{40} + \bar{c}_\psi^2 \frac{\delta_x^2}{24} \right) \right] \cos(\bar{x}_c - t) \quad (\text{B } 1c)$$

$$\ddot{\theta}' + \frac{1}{\beta\delta_z} \theta' \approx -\epsilon \bar{c}_\psi \left[ \frac{1}{\beta\delta_z} - 1 - \frac{1}{\beta\delta_z} \left( \bar{c}_\psi^2 \frac{\delta_x^2}{40} + \bar{s}_\psi^2 \frac{\delta_y^2}{24} \right) \right] \cos(\bar{x}_c - t) \quad (\text{B } 1d)$$

$$\ddot{\psi}' \approx -\epsilon \left( \frac{\delta_x^2 - \delta_y^2}{\delta_x^2 + \delta_y^2} \right) \bar{s}_\psi \bar{c}_\psi \sin(\bar{x}_c - t). \quad (\text{B } 1e)$$

The  $z'_c, \varphi'$  and  $\theta'$  equations are that of forced harmonic oscillators with natural frequencies  $\sqrt{1/\beta\delta_z}$ . Notice that for flat floaters, with  $\delta_z \ll \delta_x, \delta_y$ , we indeed have nearly the same natural oscillation frequencies  $\omega_z \approx \omega_\varphi \approx \omega_\theta \approx \sqrt{1/\beta\delta_z}$  [see the general Eqs. (3.15)]. Considering that  $\delta_z \ll 1$ , we have  $\sqrt{1/\beta\delta_z} \gg 1$ , implying that the incoming wave is never resonantly forcing the  $z'_c, \varphi'$  and  $\theta'$  oscillations. Hence, the solution for the motion is the sum of free oscillations at the bobbing frequency and a harmonic response. In the theoretical calculation, we discard all free high-frequency oscillations as such motions are strongly damped by radiative dissipation in reality.

The second order mean torque  $\bar{K}_z$  is defined in (4.21) and it split in two parts  $\bar{K}_z = \bar{K}_z^{(1)} + \bar{K}_z^{(2)}$ . To find the first part, we must reconsider the calculation of the torque

$$K_z^{(1)} = - \int_{V_{sub}^{(0)}} (s_\psi \tilde{x} + c_\psi \tilde{y}) a_x^{(1)} dV \approx \tilde{I}_{zz} (-\epsilon \Lambda s_\psi c_\psi e^{z_c} \sin(x_c - t)) \quad (\text{B } 2)$$

where  $\Lambda = (\delta_x^2 - \delta_y^2)/(\delta_x^2 + \delta_y^2)$ . To get the first and second order parts in this torque, we must evaluate this formula not a the equilibrium position, but on the trajectory of the floater  $(x_c, z_c, \psi) \approx (\bar{x}_c + x'_c, \bar{z}_c + z'_c, \bar{\psi} + \psi')$ . This generates the  $O(\epsilon^2)$  mean "drift"-like torque that we expressed in (4.21) using a Taylor expansion. Let us detail this step here.

We have

$$\begin{aligned} & \tilde{I}_{zz}^{-1} K_z^{(1)} \Big|_{(\bar{x}_c + x'_c, \bar{z}_c + z'_c, \bar{\psi} + \psi')} \\ & \approx - \underbrace{\epsilon \Lambda \bar{s}_\psi \bar{c}_\psi e^{\bar{z}_c} \sin(\bar{x}_c - t)}_{K'_z} \\ & - \epsilon \Lambda e^{\bar{z}_c} [(\bar{c}_\psi^2 - \bar{s}_\psi^2) \psi' \sin(\bar{x}_c - t) + \bar{s}_\psi \bar{c}_\psi (z'_c \sin(\bar{x}_c - t) + x'_c \cos(\bar{x}_c - t))] + O(\epsilon^3). \end{aligned} \quad (\text{B3})$$

We simplify  $e^{\bar{z}_c} = 1 + O(\delta_z)$  in the flat floater limit and inject the first order expressions of  $x'_c, z'_c, \psi'$ . Averaging over time and using

$$\overline{\psi' \sin(\bar{x}_c - t)} = \frac{\epsilon \Lambda}{2} \bar{s}_\psi \bar{c}_\psi, \quad \overline{z'_c \sin(\bar{x}_c - t) + x'_c \cos(\bar{x}_c - t)} \approx \epsilon, \quad (\text{B4})$$

we find

$$\tilde{I}_{zz}^{-1} \bar{K}_z^{(1)} \approx -\epsilon^2 \Lambda \bar{s}_\psi \bar{c}_\psi \left[ 1 + \frac{\Lambda}{2} (\bar{c}_\psi^2 - \bar{s}_\psi^2) \right] \quad (\text{B5})$$

as first part in the mean torque. This part of the torque always favors the longitudinal state.

The second part of the mean torque is the sum of three terms  $\bar{K}_z^{(2)} = \bar{T}_1 + \bar{T}_2 + \bar{T}_3$ . This notation refers here to the three separate integrals that are visible in (4.18b). The first contribution turns out to be negligible in the flat floater limit  $\delta_z \ll \delta_x, \delta_y$ . We find

$$\tilde{I}_{zz}^{-1} \bar{T}_1 \approx -\tilde{I}_{zz}^{-1} \overline{\left( \int_{V_{sub}^{(0)}} (s_\psi \theta' - c_\psi \varphi') \tilde{z} a_x^{(1)} dV \right)}_{(\bar{x}_c, \bar{z}_c, \bar{\psi})} \approx O(\epsilon^2 \delta_z) \quad (\text{B6})$$

and this will always be smaller than the other terms of order  $O(\epsilon^2)$  and  $O(\epsilon^2 \delta_x^2 / \beta \delta_z)$ . The second term is not negligible:

$$\begin{aligned} \tilde{I}_{zz}^{-1} \bar{T}_2 &= -\tilde{I}_{zz}^{-1} \overline{\left( \int_{V_{sub}^{(0)}} (s_\psi \tilde{x} + c_\psi \tilde{y}) a_x^{(2)} dV \right)}_{(\bar{x}_c, \bar{z}_c, \bar{\psi})} \\ &\approx -\tilde{I}_{zz}^{-1} \overline{\left( \int_{V_{sub}^{(0)}} (s_\psi \tilde{x} + c_\psi \tilde{y}) (-\theta' \tilde{x} + \varphi' \tilde{y}) \partial_z a_{x,c} dV \right)}_{(\bar{x}_c, \bar{z}_c, \bar{\psi})} \approx \frac{\epsilon^2 \Lambda}{2} \bar{s}_\psi \bar{c}_\psi \quad (\text{B7}) \end{aligned}$$

We detail here the part of  $a_x^{(2)}$  that creates the leading contribution. This term captures the small torque that is created by small vertical gradients in wave-magnitude ( $\partial_z a_{x,c}$ ) along its elongated surface and due to rotations ( $\theta'$  and  $\varphi'$ ). The term alone creates a slow  $O(\epsilon^2)$  motion that would rather be in favor of the transverse position. However, it can never dominate the other  $O(\epsilon^2)$  terms in the  $\bar{K}_z^{(1)}$  mean torque.

The third contribution to  $\bar{K}_z^{(2)}$  is the longest to evaluate. In the flat floater limit, we

find it as

$$\begin{aligned}
 \tilde{I}_{zz}^{-1} \bar{T}_3 &= -\tilde{I}_{zz}^{-1} \left( \int_{V_{sub}^{(1)}} (s_\psi \tilde{x} + c_\psi \tilde{y}) a_x^{(1)} dV \right)_{(\bar{x}_c, \bar{z}_c, \bar{\psi})} \\
 &\approx \frac{\epsilon e^{z_c} \cos(x_c - t)}{\beta \delta_z (\delta_x^2 + \delta_y^2)} \left[ s_\psi \underbrace{(\theta' + \epsilon c_\psi \cos(x_c - t))}_{\delta_x^2} - c_\psi \underbrace{(\varphi' + \epsilon s_\psi \cos(x_c - t))}_{\delta_y^2} \right. \\
 &\quad \left. + \left( c_\psi^3 s_\psi \left( -\frac{\delta_x^4}{40} + \frac{\delta_x^2 \delta_y^2}{24} \right) - s_\psi^3 c_\psi \left( -\frac{\delta_y^4}{40} + \frac{\delta_x^2 \delta_y^2}{24} \right) \right) \epsilon \cos(x_c - t) \right] \\
 &+ \frac{\epsilon e^{z_c} \sin(x_c - t)}{\beta \delta_z (\delta_x^2 + \delta_y^2)} \left[ s_\psi c_\psi (\delta_x^2 - \delta_y^2) \underbrace{(z'_c - \epsilon \sin(x_c - t))}_{\delta_x^2} \right. \\
 &\quad \left. + \left( c_\psi^3 s_\psi \left( 3 \frac{\delta_x^4}{40} - 2 \frac{\delta_x^2 \delta_y^2}{24} \right) - s_\psi^3 c_\psi \left( 3 \frac{\delta_y^4}{40} - 2 \frac{\delta_x^2 \delta_y^2}{24} \right) \right) \epsilon \sin(x_c - t) \right]. \quad (\text{B } 8)
 \end{aligned}$$

Physically, this term captures on its own the torque that is due to the changing submersion of the floater (integral over  $V_{sub}^{(1)}$ ). The underbraced terms show more clearly how the first order motion  $z'_c, \theta', \varphi'$  influences this varying submersion and hence this torque. Quite astonishingly, we observe that the first term exactly vanishes after injecting the solutions of  $\theta'$  and  $\varphi'$ , even with the tiny  $O(\epsilon \delta_x^2, \epsilon \delta_y^2)$  corrections. Hence, we can deduce that these weak corrections in  $\theta'$  and  $\varphi'$  are in fact not so relevant in this problem. The second term does not vanish. After injecting the  $z'_c$ -motion, we find that the very small  $O(\epsilon \delta_x^2, \epsilon \delta_y^2)$  are crucially important. From (4.25b), we get that

$$z'_c - \epsilon \sin(\bar{x}_c - t) = -\frac{\epsilon}{24} (\bar{c}_\psi^2 \delta_x^2 + \bar{s}_\psi^2 \delta_y^2) \sin(\bar{x}_c - t). \quad (\text{B } 9)$$

The right hand side may seem tiny, but without these terms, we would simply find  $\bar{T}_3 = 0$ . Hence, these weak buoyancy-induced corrections of the vertical motion are crucial and the only ones that can cause  $\bar{T}_3$  to be non-zero in this model, at this order. After taking the time-average, we find

$$\tilde{I}_{zz}^{-1} \bar{T}_3 \approx \frac{\epsilon^2}{\beta \delta_z (\delta_x^2 + \delta_y^2)} \left[ \bar{s}_\psi \bar{c}_\psi^3 \left( \frac{\delta_x^4}{60} - \frac{\delta_x^2 \delta_y^2}{48} \right) - \bar{s}_\psi^3 \bar{c}_\psi \left( \frac{\delta_y^4}{60} - \frac{\delta_x^2 \delta_y^2}{48} \right) \right]. \quad (\text{B } 10)$$

Without considering the anisotropy of the floater, this term causes a contribution of  $O(\epsilon^2 \delta)$  to the motion of  $\bar{\psi}$  that in fact, seems smaller than the other mean torques of order  $O(\epsilon^2)$ . However, for strongly elongated floaters with  $\delta_x \gg \delta_y \gg \delta_z$ , this term is rather of magnitude  $O(\epsilon^2 \delta_x^2 / \beta \delta_z)$  and dominates the  $O(\epsilon^2)$  terms. In our calculations, we were able to retrace that this term  $\bar{T}_3$  was entirely due to the existence of a non-zero curvature of the water-line at the floater position (the term  $(1/2)(x - x_c)^2 \partial_{xx}^2 \zeta_c$  in the Taylor expansion for  $\tilde{\zeta}$ ) and it is this physical element that brought us to the simplified model discussed in section 5.

In the end, we have summed up all the contributions to the second order mean torque. Expressing  $\tilde{I}_{zz}^{-1} \ddot{\bar{\psi}} = \bar{K}_z$ , we then found the equation of motion (4.26).

## REFERENCES

ABRAMOWITZ, MILTON & STEGUN, IRENE A 1948 *Handbook of mathematical functions with formulas, graphs, and mathematical tables*, , vol. 55. US Government printing office.

- VAN DEN BREMER, T. S. & BREIVIK, Ø. 2018 Stokes drift. *Philosophical Transactions of the Royal Society A: Mathematical, Physical and Engineering Sciences* **376** (2111), 20170104.
- BUREAU-VERITAS 2016 Hydrostar for experts user manual. *Bureau Veritas* .
- BUTIKOV, E.I. 2001 On the dynamic stabilization of an inverted pendulum. *Am. J. Phys* **69**, 1–14.
- CALVERT, R., McALLISTER, M. L., WHITTAKER, C., RABY, A., BORTHWICK, A.G.L. & VAN DEN BREMER, T.S. 2021 A mechanism for the increased wave-induced drift of floating marine litter. *Journal of Fluid Mechanics* **915**, A73.
- CHEN, XIAO-BO 2007 Middle-field formulation for the computation of wave-drift loads. *Journal of Engineering Mathematics* **59** (1), 61–82.
- CLARK, LAURA K., DiBENEDETTO, MICHELLE H., OUELLETTE, NICHOLAS T. & KOSEFF, JEFFREY R. 2020 Settling of inertial nonspherical particles in wavy flow. *Physical Review Fluids* **5** (12), 124301.
- DiBENEDETTO, MICHELLE H., CLARK, LAURA K. & PUJARA, NIMISH 2022 Enhanced settling and dispersion of inertial particles in surface waves. *Journal of Fluid Mechanics* **936**, A38.
- DiBENEDETTO, MICHELLE H., KOSEFF, JEFFREY R. & OUELLETTE, NICHOLAS T. 2019 Orientation dynamics of nonspherical particles under surface gravity waves. *Physical Review Fluids* **4** (3), 034301.
- DiBENEDETTO, MICHELLE H. & OUELLETTE, NICHOLAS T. 2018 Preferential orientation of spheroidal particles in wavy flow. *Journal of Fluid Mechanics* **856**, 850–869.
- DiBENEDETTO, MICHELLE H., OUELLETTE, NICHOLAS T. & KOSEFF, JEFFREY R. 2018 Transport of anisotropic particles under waves. *Journal of Fluid Mechanics* **837**, 320–340.
- FALNES, JOHANNES & KURNIAWAN, ADI 2020 *Ocean waves and oscillating systems: linear interactions including wave-energy extraction*, , vol. 8. Cambridge university press.
- FALTINSEN, ODD 1993 *Sea loads on ships and offshore structures*, , vol. 1. Cambridge university press.
- FALTINSEN, ODD MAGNUS 1980 Prediction of resistance and propulsion of a ship in a seaway. In *13th Symposium on Naval Hydrodynamics, Tokyo*, pp. 505–529.
- JEFFERY, G.B. 1922 The motion of ellipsoidal particles immersed in a viscous fluid. *Soc. Lond. A* **102**, 161–179.
- KAPITZA, P.L. 1951 Pendulum with an oscillating pivot. *Sov. Phys. Uspekhi* **44**, 7–20.
- KASHIWAGI, M 1992 Added resistance, wave-induced steady sway force and yaw moment on an advancing ship. *Schiffstechnik* **39**, 3–16.
- KASHIWAGI, MASASHI & OHKUSU, MAKOTO 1993 Study on the wave-induced steady force and moment. *Journal of The Society of Naval Architects of Japan* **1993** (173), 185–194.
- LANDAU, L.D. & LIFSHITZ, E. M. 1960 *Course of Theoretical Physics: Mechanics*. Pergamon Press.
- LE BOULLUEC, MARC, FOREST, BERTRAND & MANSUY, EMMANUEL 2008 Steady drift of floating objects in waves - experimental and numerical investigations. *Proceedings of the ASME 27th International Conference on Offshore Mechanics and Arctic Engineering* .
- NEWMAN, JOHN NICHOLAS 1967 The drift force and moment on ships in waves. *Journal of ship research* **11** (01), 51–60.
- NEWMAN, JOHN NICHOLAS 2018 *Marine hydrodynamics*. The MIT press.
- SALVESEN, NILS 1974 Second order steady state forces and moments on surface ships in oblique regular waves. In *Naval Ship Research and Development Center, Washington DC, USA, Proceedings of the International Symposium on the Dynamics of Marine Vehicles and Structures in Waves, University College London, Paper 22*, pp. 225–241.
- SKEJIC, RENATO & FALTINSEN, ODD M 2008 A unified seakeeping and maneuvering analysis of ships in regular waves. *Journal of marine science and technology* **13**, 371–394.
- SPENS, PAUL G & LALANGAS, PETROS A 1962 Measurements of the mean lateral force and yawing moment on a series 60 model in oblique regular waves. *Tech. Rep.*. Stevens Inst. of Technology, Davidson Laboratory.
- STOKES, G. G. 1847 On the theory of oscillatory waves. *Trans. Camb. Phil. Soc.* **8**, 441–455.
- SUARIA, G., BERTA, M., GRIFFA, A., MOLCARD, A., ÖZGÖKMEN, T. M., ZAMBIANCHI, E. & ALIANI, S. 2021 Dynamics of transport, accumulation, and export of plastics at oceanic fronts. *Chemical Oceanography of Frontal Zones* p. 355–405.



- SUTHERLAND, BRUCE R, DiBENEDETTO, MICHELLE, KAMINSKI, ALEXIS & VAN DEN BREMER, TON 2023 Fluid dynamics challenges in predicting plastic pollution transport in the ocean: A perspective. *Physical Review Fluids* **8** (7), 070701.
- SUYEHIRO, K 1921 The yawing of ships caused by the oscillation amongst waves. *Journal of Zosen Kiokai* **1920** (26), 23–33.
- YANG, M., ZHANG, B., CHEN, X., KANG, Q., GAO, B., LEE, J. & B., CHEN 2023 Transport of microplastic and dispersed oil co-contaminants in the marine environment. *Environ. Sci. Technol.* **57**, 5633–5645.
- YASUKAWA, HIRONORI, HIRATA, NORITAKA, MATSUMOTO, AKINORI, KUROIWA, RYOTA & MIZOKAMI, SHUJI 2019 Evaluations of wave-induced steady forces and turning motion of a full hull ship in waves. *Journal of marine science and technology* **24**, 1–15.